Articles

Probing the Ser-Ser-Lys Catalytic Triad Mechanism of Peptide Amidase: Computational Studies of the Ground State, Transition State, and Intermediate†

Anna Liza B. Valiña,‡ Devleena Mazumder-Shivakumar,‡ and Thomas C. Bruice*

Department of Chemistry and Biochemistry, University of California, Santa Barbara, California 93106

Received May 13, 2004; Revised Manuscript Received September 3, 2004

ABSTRACT: Peptide amidase (Pam), a hydrolytic enzyme that belongs to the amidase signature (AS) family, selectively catalyzes the hydrolysis of the C-terminal amide bond ($CO-NH_2$) of peptides. The recent availability of the X-ray structures of Pam, fatty acid amide hydrolase, and malonamidase E2 has led to the proposal of a novel Ser-Ser-Lys catalytic triad mechanism for the amide hydrolysis by the AS enzymes. The molecular dynamics (MD) simulations using the CHARMM force field were performed to explore the catalytic mechanism of Pam. The 1.8 Å X-ray crystal structure of Pam in complex with the amide analogue of chymostatin was chosen for the initial coordinates for the MD simulations. The five systems that were investigated are as follows: (i) enzyme·substrate with Lys123-NH_2, (ii) enzyme·substrate with Lys123-NH_3^+, (iii) enzyme·substrate with Lys123-NH_3^+ and Ser226-O^-, (iv) enzyme·transition state, and (v) enzyme·tetrahedral intermediate. Our data support the presence of the hydrogen bonding network among the catalytic triad residues, Ser226, Ser202, and Lys123, where Ser226 acts as the nucleophile and Ser202 bridges Ser226 and Lys123. The MD simulation supports the catalytic role of the crystallographic waters, Wat1 and Wat2. In all the systems that have been studied, the backbone amide nitrogens of Asp224 and Thr223 create an oxyanion hole by hydrogen bonding to the terminal amide oxygen of the substrate, and stabilize the oxyanion tetrahedral intermediate. The results from both our computational investigation and previously published experimental pH profile support two mechanisms. In a mechanism that is relevant at lower pH, the Lys123-NH_3^+-Ser202 dyad provides structural support to the catalytic residue Ser226, which in turn carries out a nucleophilic attack at the substrate amide carbonyl in concert with Wat1-mediated deprotonation and stabilization of the tetrahedral transition state by the oxyanion hole. In the mechanism operating at higher pH, the Lys123-NH_2-Ser202 catalytic dyad acts as a general base to assist addition of Ser226 to the substrate amide carbonyl. The results from the MD simulation of the tetrahedral intermediate state show that both Ser202 and Lys123 are possible candidates for protonation of the leaving group, NH_2, to form the acyl−enzyme intermediate.

Peptide amidase (Pam)[1] is a hydrolytic enzyme that belongs to the amidase signature (AS) family. The AS family is characterized by a highly conserved C-terminal region that is rich in serine and glycine residues (*1*, *2*). The biochemical functions and substrate specificities of these AS enzymes vary widely even though their common catalytic function is the hydrolysis of the amide bond ($CO-NH_2$). The AS sequence is devoid of aspartic acid and histidine. Thus, the AS enzymes do not belong to the classical serine hydrolases that include most serine proteases, lipases, and esterases which employ the Ser-His-Asp catalytic triad (*3*).

The catalytic mechanism of the fatty acid amide hydrolase (FAAH) from *Rattus norvegicus* as determined by site-directed mutagenesis, affinity labeling, and steady state kinetic methods led to the postulation that AS family enzymes are Ser-Lys dyad hydrolases (*4*−*6*) (Scheme 1A). The mechanism involved Lys142-NH_2 (similar to Lys123 in Pam) as the general base that activates the nucleophilic Ser241 (similar to Ser226 in Pam) via the bridging residue Ser217 (similar to Ser202 in Pam). The species Lys142-NH_2 was proposed to be present in the active site based on mutagenesis results.

The recent availability of X-ray structures of three AS enzymes [Pam, FAAH, and MAE2 (malonamidase E2)] has led to the proposal of a novel Ser-Ser-Lys catalytic triad mechanism for the amide hydrolysis by the AS enzymes (Scheme 1B). Though the Ser-Ser-Lys catalytic residues are highly conserved among these AS enzymes, the proposed mechanism for each of the crystallized enzymes differs in the formation of the covalent acyl−enzyme intermediate (*7*−*9*). In Scheme 1B, Ser226 acts as the primary nucleophile

† This study was supported by National Science Foundation Grant MCB-0129568.

* To whom correspondence should be addressed. Phone: (805) 893-2044. Fax: (805) 893-2229. E-mail: tcbruice@chem.ucsb.edu.

‡ These authors contributed equally to this work.

[1] Abbreviations: Pam, peptide amidase; Cst, chymostatin; Cst-NH_2, amide analogue of chymostatin; AS, amidase signature; MAE2, malonamidase E2; FAAH, fatty acid amide hydrolase; NAC, near-attack conformer; TS, transition state; In, intermediate; MD, molecular dynamics; rmsd, root-mean-square deviation; SB, stochastic boundary; PB, periodic boundary; RESP, restrained electrostatic potential.

10.1021/bi049025r CCC: $27.50
Published on Web 11/23/2004

Scheme 1: Proposed Mechanism of FAAH (*8*)

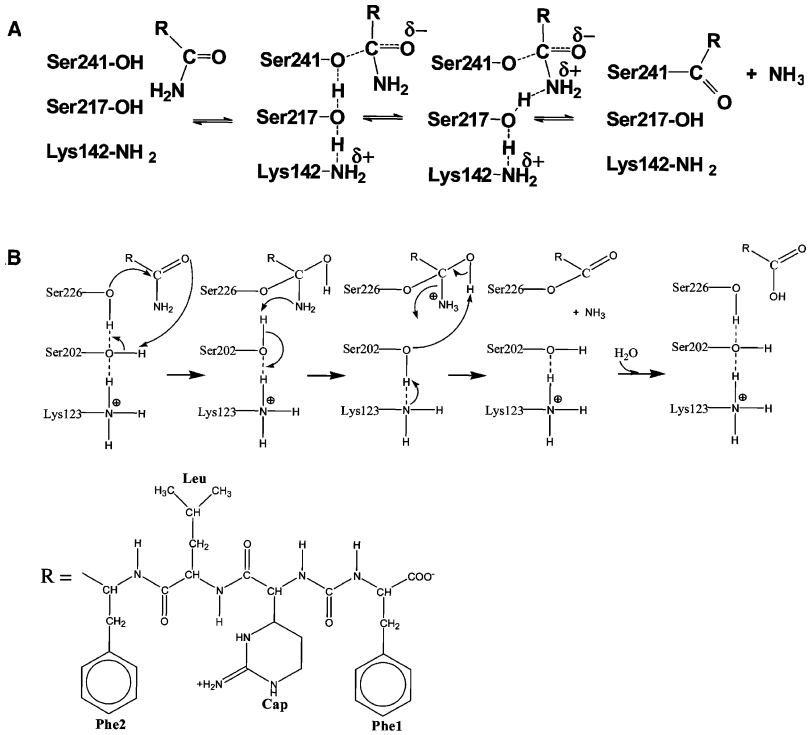

that attacks the amide carbonyl carbon atom. In this mechanism, the bridging residue Ser202, between Lys123 and Ser226, acts as a general acid−general base catalyst by simultaneously protonating the substrate's carbonyl oxygen and abstracting a proton from Ser226-OH to activate this nucleophile (*9*). In the second step of Scheme 1B, Lys123-NH_3^+, which is directly in contact with Ser202-OH, is proposed to donate a proton to Ser202, thus acting as an acid catalyst. This role of Lys123-NH_3^+ in Pam (Scheme 1B) is in contrast to the study of FAAH (Scheme 1A) in which the catalytic lysine residue was proposed to function as a base catalyst in both the Ser-Lys catalytic dyad and the Ser-Ser-Lys triad mechanism (*4*, *5*, *8*).

This study is focused on understanding the catalytic mechanism of Pam. Pam isolated from *Stenotrophomonas maltophilia*, a Gram-negative bacterium, selectively catalyzes the hydrolysis of the C-terminal amide bond of peptides. The selectivity of peptide amidases is useful in biotechnological applications such as deprotonation of peptide amides during in vitro synthesis of peptide hormones with a C-terminal amidation (*10*, *11*). The biological substrate of Pam remains unidentified.

Despite the supporting evidence for a Ser-Ser-Lys triad mechanism for Pam, additional study is required to assess just what this mechanism is. Computational simulations have been carried out in an effort to obtain a description of the plausible reactive species for the serine-mediated nucleophilic attack and to map out proton abstraction and transfer among the Ser-Ser-Lys catalytic triad. The transition state and intermediate were modeled to provide the steric criteria for the nucleophilic addition reaction. Analysis of long-term MD simulations has provided useful data about the covalent acyl−enzyme intermediate, protonation of the leaving group, and the collapse of the tetrahedral intermediate. Long-term MD simulations have been performed on the ground states (E·S, EH·S, and E^-H·S), the transition state (E·TS), and the intermediate state (E·In) to elucidate the catalytic mechanism of Pam (Chart 1).

MATERIALS AND METHODS

The 1.8 Å X-ray crystal structure of the enzyme peptide amidase (Pam) in complex with its competitive inhibitor chymostatin (Cst) [PDB entry 1M21 (*9*)] was chosen for the initial coordinates for the MD simulations (Figure 1). The

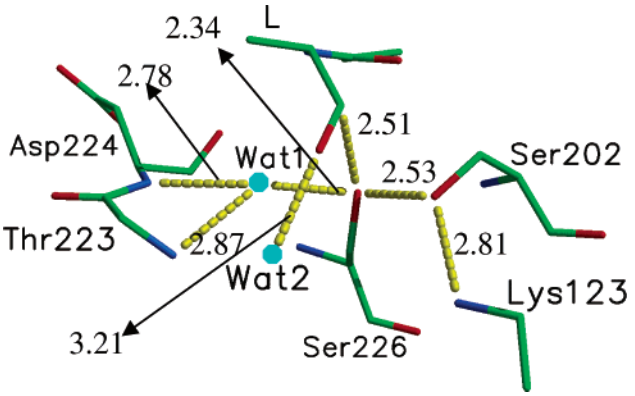

FIGURE 1: Position of active site residues from X-ray crystal structure. Note the orientation of Wat1 and Wat2 (cyan). The distances are measured from the X-ray crystal structure (PDB entry 1M21) and are in angstroms. L represents Cst.

X-ray crystal structure shows two crystallographic water molecules (Wat1 and Wat2) in the active site (Figure 1). The substrate structure was modeled from Cst by replacing the aldehyde −C(═O)H group with the amide −(C═O)NH_2 group. The amide analogue of chymostatin is termed Cst-NH_2 (see Scheme 1A). CHARMM 27 (*12*) residue topology and parameter files were employed to describe force fields for the proteins, substrate, and TIP3P water model (*12*). All MD simulations were run using CHARMM. Missing tor-

Chart 1.[a]

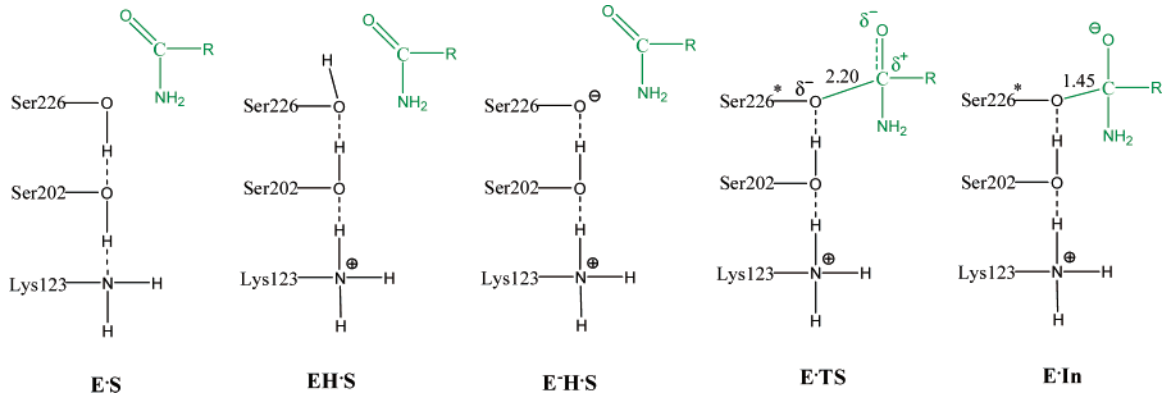

[a] Ser226* is a part of the transition state (TS) and the intermediate (In) in E·TS and E·In and, therefore, is termed Ser226* in E·TS and E·In. The structure of R is shown in Scheme 1A.

Chart 2

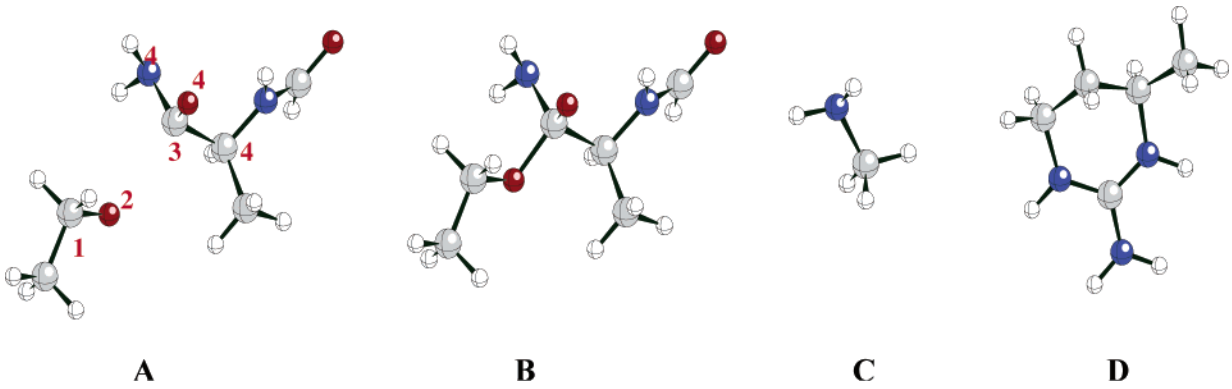

sional parameters and atomic charges for the substrate, transition state, and intermediate structure were generated using quantum mechanics (*vide infra*).

MD Simulations. MD simulations were carried out for the five systems (E·S, EH·S, E⁻H·S, E·TS, and E·In) displayed in Chart 1. Hydrogens were added with the HBUILD (*13*) module in CHARMM. All Glu, Asp, Lys, and Arg residues were charged, unless otherwise specified. In the E·S ground state, Lys123 is neutral (Lys123-NH_2). The enzyme·substrate system was solvated in an equilibrated TIP3P water box with dimensions of 80 Å × 80 Å × 72 Å using the center of mass of the enzyme as the origin. Any solvent molecule within 2.8 Å of a heavy atom of the enzyme was deleted. Minimization and equilibration of the solvent molecules (39 228 atoms) were carried out at 300 K for 3 ps while the enzyme, substrate, and crystallographic water molecules were kept fixed to achieve a favorable distribution of water molecules on the enzyme surface. The solvated enzyme·substrate systems were prepared for MD simulations by first applying 100 steps of energy minimization using the steepest descent (SD) method followed by 100 steps of the adopted basis Newton−Raphson (ABNR) method (*12*).

Molecular Parameters and Modeling of the Transition State and Intermediate. The models for the transition state (Chart 2A) and the intermediate (Chart 2B) were optimized at the B3LYP/6-31+G(d,p) and MP2/6-31+G(d,p) levels of theory, respectively, using Gaussian 98 (*14*). The electrostatic potential for the transition state (TS) was calculated at the MP2/6-31+G(*) level. The electrostatic potentials for the intermediate (In), neutral lysine (Chart 2C), and the Cap ring of Cst-NH_2 (Chart 2D) were calculated at the B3LYP/3-21+G(*) level. Restrained electrostatic potential (RESP) fitting of point charges to these electrostatic potentials was used to calculate partial atomic charges (*15*). Missing molecular parameters that include bond distances and angle parameters were taken directly from the optimized structures. The CHARMM force field (*12*) does not have the torsional parameters for describing the rotations around the CO−CX bond (where X is N, O, or Cα) for both the intermediate and the transition state. The C, O, C, and X atoms are labeled 1−4, respectively, in Chart 2A. Conformation analysis with a quantum mechanical method was performed with a model compound (Chart 2A) to obtain this missing torsional parameter that describes the bonding of the nucleophilic hydroxyl oxygen of Ser226 to the electrophilic carbonyl carbon of the substrate. CHARMM was then used to calculate these conformational energies, and the CHARMM parameters were adjusted until a good agreement was reached between the CHARMM and *ab initio* data.

Prediction of the Structure of NAC. The structure of NAC was predicted on the basis of the structure of TS (Chart 2A) predicted by *ab initio* methods. The angle in the *ab initio* TS was 113°. The van der Waals parameters for the NAC criteria were taken from ref *23*.

Periodic Boundary Setup. Periodic boundary molecular dynamics simulations (PBMD) at constant pressure and temperature for 300 ps with an integration time step of 0.0015 ps were performed on both E·S and EH·S ground state systems. The SHAKE algorithm (*16*) was applied to constrain the bonds containing hydrogens to their equilibrium length.

Integration of the equation of motion was done by using the Verlet leapfrog algorithm (*17*). The disadvantage of using this algorithm is that the positions and velocities are not synchronized. However, the leapfrog algorithm is a popular choice for algorithms used for MD simulations. The nonbonded list was updated every 20 time steps, and a cutoff of 12 Å was used for the nonbonded interactions. The Coulombic term was cut off by using a force-shifting function, and the Lennard-Jones term was cut off with a switching function. Initially, the system was coupled to a 200 K heat bath for 15 ps using a coupling constant of 5.0 ps. For the rest of the simulation, the system was subsequently coupled to a 300 K heat bath using a coupling constant of 5.0 ps. The constant pressure was maintained by the Berendsen algorithm (*18*) using an isothermal compressibility of 4.63 $\times$ 10^{-5} atm^{-1} and a pressure coupling constant of 5.0 ps. Coordinates from the MD simulations were saved every 100 time steps. For the E·S system, initial harmonic constraints were applied to the catalytic residues for the first 100 ps of the dynamics to direct the hydrogen bonding as shown in Chart 1.

Stochastic Boundary Setup. The large dimension of the E·S and EH·S systems under periodic boundary (PB) conditions is computationally expensive. Therefore, stochastic boundary conditions (SB) were applied after equilibrating the systems for 300 ps using periodic boundary conditions. The periodic box systems of the E·S and EH·S systems were reduced to spherical TIP3P-solvated enzyme·substrate systems with radii of 25 Å. Each system was separated into a reaction zone that consists of a reaction region (r < 23 Å using the electrophilic carbonyl carbon of the substrate Cst-NH_2 as the origin), a buffer region (23 Å < r < 25 Å), and a reservoir region (r > 25 Å). Harmonic constraint was used to fix all protein atoms in the reservoir region, while all water molecules in this region were deleted. Overall, E·S, EH·S, E^-H·S, E·TS, and E·In have 8066 (2694 water atoms), 7980 (2385 water atoms), 7946 (2694 water atoms), 7953 (2694 water atoms), and 7966 atoms (2691 water atoms), respectively. Each system was energy-minimized with the SD method (100 steps for E·S and EH·S and 500 steps for E·In, E^-H·S, and E·TS) followed by 500 steps of the ABNR method followed by each system being heated to 300 K for 30 ps.

During simulations, atoms in the reaction region are treated with molecular dynamics. Heavy atoms found in the buffer region undergo langevine dynamics, and were constrained by harmonic restoring force with force constants derived from their average Debye−Waller factors (*19*). Water molecules were confined by deformable boundary conditions to the active site region (*20*). The system was coupled to a heat bath of 300 K using a frictional coefficient of 250 ps^{-1} on the protein heavy atoms and 62 ps^{-1} on the TIP3P water molecules. The SHAKE algorithm (*16*) was used to fix bonds containing hydrogen atoms. The stochastic boundary molecular dynamics (SBMD) (*19*) was performed using a constant pressure and temperature, and a time step of 0.001 ps to integrate the equations of motion.

Preliminary MD of the E·S system showed that the nucleophilic hydroxyl oxygen of Ser226-OH drifted away from the electrophilic carbonyl carbon atom of Cst-NH_2. Thus, a distance constraint of 3.2 Å was applied for 400 ps between the amide carbonyl carbon and Ser226-OH, with a force constant of 100 kcal mol^{-1} $Å^{-2}$ in the E·S system. In the E·In model, the distance between the terminal amide nitrogen of NH_2 of the substrate and the hydroxyl oxygen of Ser202-OH was constrained at 2.8 Å using a force constant of 50 kcal mol^{-1} $Å^{-2}$ for the first 400 ps. The total time periods for the SBMD simulations for E·S, EH·S, E^-H·S, E·TS, and E·In systems were 14, 16, 2, 10, and 10 ns, respectively. Analysis of the production dynamics was performed for the final 8 ns for E·S, 800 ps for E^-H·S, 6 ns for EH·S and E·TS, and 4 ns for E·In.

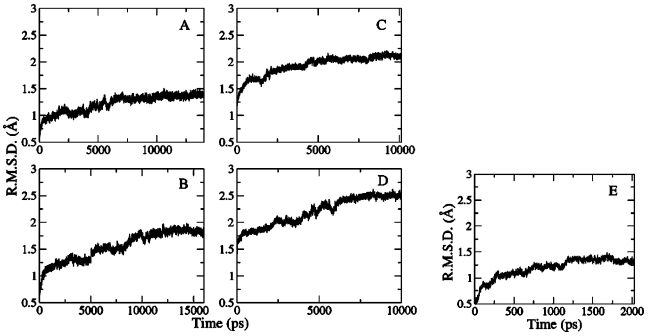

FIGURE 2: Root-mean-square deviation of backbone heavy atoms (Cα, N, C, and O) vs time of MD simulations for (A) the E·S system for 14 ns, (B) the EH·S system for 16 ns, (C) the E·TS system for 10 ns, (D) the E·In system for 10 ns, and (E) the E^-H·S system for 2 ns.

RESULTS

The long-term MD simulations of the five systems depicted in Chart 1 are described in this section. Three ground states for Pam (E·S, EH·S, and E^-H·S) were modeled (Chart 1), and their dynamics were compared to determine which ground state best represents the reactive species. The E·S system consists of neutral Lys123 (Lys123-NH_2), while the EH·S system consists of protonated Lys123 (Lys123-NH_3^+). The E^-H·S system also has Lys123-NH_3^+, but E^-H·S differs from the other ground states in that it has a deprotonated nucleophile, Ser226-O^-. After activation of the nucleophile, Ser226-OH, these ground states would form the same tetrahedral intermediate. E·TS and E·In depict the tetrahedral acyl−enzyme transition state and intermediate, respectively.

Stability of Dynamics

The MD simulations were carried out for 14 and 16 ns for E·S (Figure 2A) and EH·S (Figure 2B), respectively, 2 ns for E^-H·S, and 10 ns for both E·TS (Figure 2C) and E·In (Figure 2D). The root-mean-square deviations (rmsds) of the backbone heavy atoms (Cα, N, C, and O) of the enzyme with respect to the energy-minimized structure are used to determine the structural stability of the system (Figure 2). The E·S, EH·S, E·TS, and E·In systems equilibrate or reach a plateau after 6, 10, 4, and 6 ns, respectively. The average rmsds for the equilibrated E·S, EH·S, E·TS, and E·In systems are 1.34 ± 0.05, 1.82 ± 0.06, 2.06 ± 0.05, and 2.47 ± 0.05 Å, respectively. The average rmsd of E^-H·S for the last 800 ps is 1.35 ± 0.04 Å.

Population of the Reactive Species in E·S, EH·S, and E−H·S Systems

The concept of near-attack conformers (NACs) can be used as a measure of the reactive Michaelis conformers in each

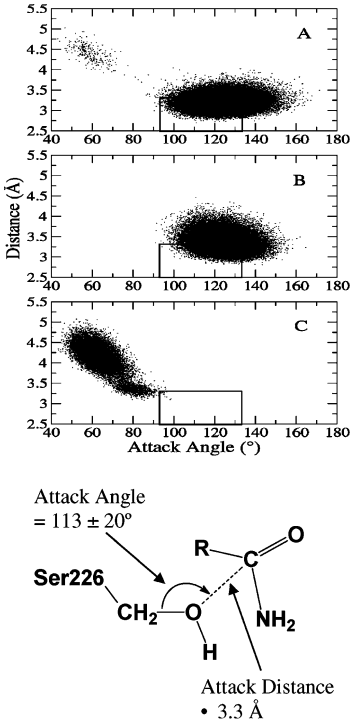

FIGURE 3: NAC plot showing the attacking distance (angstroms) vs attacking angle (degrees) for the (A) E·S, (B) EH·S, and (C) $E^{-}H$·S systems. The distance (*y*-axis) is measured between the hydroxyl oxygen of Ser226-OH and the electrophilic amide carbonyl carbon atom of Cst-NH_2. The attack angle (*x*-axis) is defined by the angle made by the carbon adjacent to the hydroxyl oxygen, the hydroxyl oxygen of Ser226-OH, and the electrophilic carbonyl carbon of the substrate. Inside the red box is the population of NACs or the reactive species. The structure shows the definition of NAC.

ground state (E·S, EH·S, and $E^{-}H$·S). NACs are the ground state conformers through which reactants pass to reach a given transition state during the formation of a covalent bond (*21*, *22*). Reactive species can be defined by two parameters (specific range of distance and angle) that are critical for a reaction to occur. The NACs for the formation of the acyl−enzyme tetrahedral intermediate have two reacting moieties (the nucleophilic hydroxyl oxygen of Ser226 and the electrophilic amide carbonyl carbon of Cst-NH_2) within the van der Waals contact distance of ≤3.33 Å (*23*) and an approaching angle of 113 ± 20°. The percentages of time that the Michaelis complex exists as a NAC for the nucleophilic addition reaction for E·S (Figure 3A), EH·S (Figure 3B), and $E^{-}H$·S (Figure 3C) are 68.3, 31.0, and 0.1%, respectively.

MD Simulations of the E·S Ground State (with Lys123-NH_2)

Polar Interactions within the Active Site of the E·S System. Chart 3A displays the hydrogen bonding interactions with Cst-NH_2 and the catalytic residues for the average MD simulations of the E·S system. Throughout the MD simulations, Ser226 is the only catalytic residue that makes contact with the reactive amide carbonyl carbon of the substrate. Ser202-OH is tightly hydrogen bonded to the amino group of Lys123-NH_2 ($R_{O\cdots N}$ = 2.79 ± 0.09 Å and $R_{H\cdots N}$ = 1.87 ± 0.10 Å), maintaining Ser202 as the bridging residue between Ser226 and Lys123. The hydroxyl oxygen of Ser226-OH is 3.18 ± 0.17 Å from the carbonyl carbon for

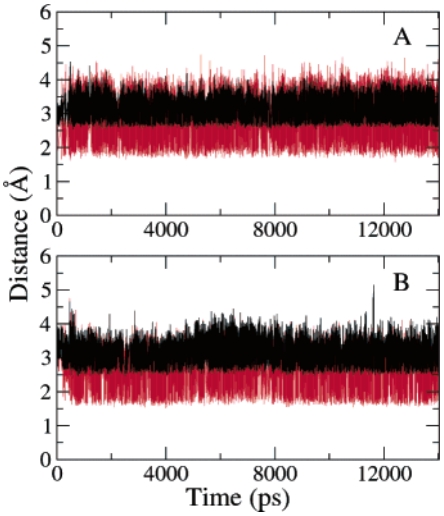

FIGURE 4: Histogram for the E·S system showing hydrogen bond distances in angstroms between (A) the hydroxyl oxygen of Ser226-OH and the hydroxyl oxygen of Ser 202-OH and (B) the hydroxyl oxygen of Ser226-OH and the terminal amide oxygen of Cst-NH_2. The black lines represent heavy atom distances and red lines those between an electronegative atom and a hydrogen atom.

nucleophilic addition. Initially, the hydroxyl group of Ser226-OH is only hydrogen bonded to Ser202-OH. After 500 ps, the hydroxyl hydrogen of Ser226-OH becomes alternatively hydrogen bonded to the hydroxyl oxygen of Ser202-OH ($R_{O\cdots O}$ = 3.11 ± 0.25 Å and $R_{OG\cdots H}$ = 2.73 ± 0.60 Å) and then the terminal carbonyl oxygen of Cst-NH_2 ($R_{O\cdots O}$ = 3.12 ± 0.30 Å and $R_{O\cdots H}$ = 2.62 ± 0.55 Å) as shown in Chart 3A and Figure 4. The amide hydrogen of Ser202 is 2.02 ± 0.16 Å from the hydroxyl oxygen of Ser226-OH, providing a strong hydrogen bonding between the two heavy atoms ($R_{O\cdots O}$ = 2.99 ± 0.15 Å).

After 500 ps, the amide hydrogens of Asp224 and Thr223 along with the hydroxyl hydrogen of Ser226-OH are hydrogen bonded to the terminal amide carbonyl oxygen of the substrate. The hydrogen bond formed by Asp224 with the substrate terminal amide oxygen is more stable with a heavy atom distance of 2.92 ± 0.17 Å ($R_{O\cdots H}$ = 1.93 ± 0.16 Å) as compared to Thr223 with a heavy atom distance of 3.71 ± 0.31 Å ($R_{O\cdots H}$ = 2.86 ± 0.37 Å). Ser226 is held in position by Ser203 and Asp224. The hydroxyl hydrogen of Ser203-OH makes a strong and stable hydrogen bond with the backbone carbonyl oxygen of Ser226 ($R_{O\cdots O}$ = 2.77 ± 0.13 Å and $R_{O\cdots H}$ = 1.88 ± 0.16 Å). The backbone oxygen of Asp224 is weakly hydrogen bonded to the amide hydrogen of Ser226 ($R_{O\cdots N}$ = 3.26 ± 0.24 Å).

Both the amide hydrogen of Ser168 and that of Ser204 are hydrogen bonded to the amide backbone oxygen of Ser202, stabilizing the cis conformation of Ser202, with the following heavy atom distances: $R_{O\cdots N}$ = 3.33 ± 0.21 Å and $R_{O\cdots N}$ = 2.87 ± 0.11 Å, respectively. Lys123-NH_2 is positioned close to Ser202 by two conserved residues, Ser203 and Thr221. The amine hydrogens of Lys123-NH_2 make stable hydrogen bonds with the hydroxyl oxygens of Ser 203-OH ($R_{O\cdots H}$ = 2.09 ± 0.20 Å) and Thr221-OH ($R_{O\cdots H}$ = 2.03 ± 0.19 Å).

The hydrogen bonds to Cst-NH_2 in the E·S system are shown in Figure 5. The terminal amide NH_2 group of the substrate is hydrogen bonded to the amide oxygen of Ala171 ($R_{O\cdots H}$ = 1.98 ± 0.17 Å). The amide hydrogen of Asn172

Chart 3: Hydrogen Bonding Distances to the Substrate and the Catalytic Residues for (A) E·S, (B) EH·S, (C) Et·S, and (D) E·In Systems[a]

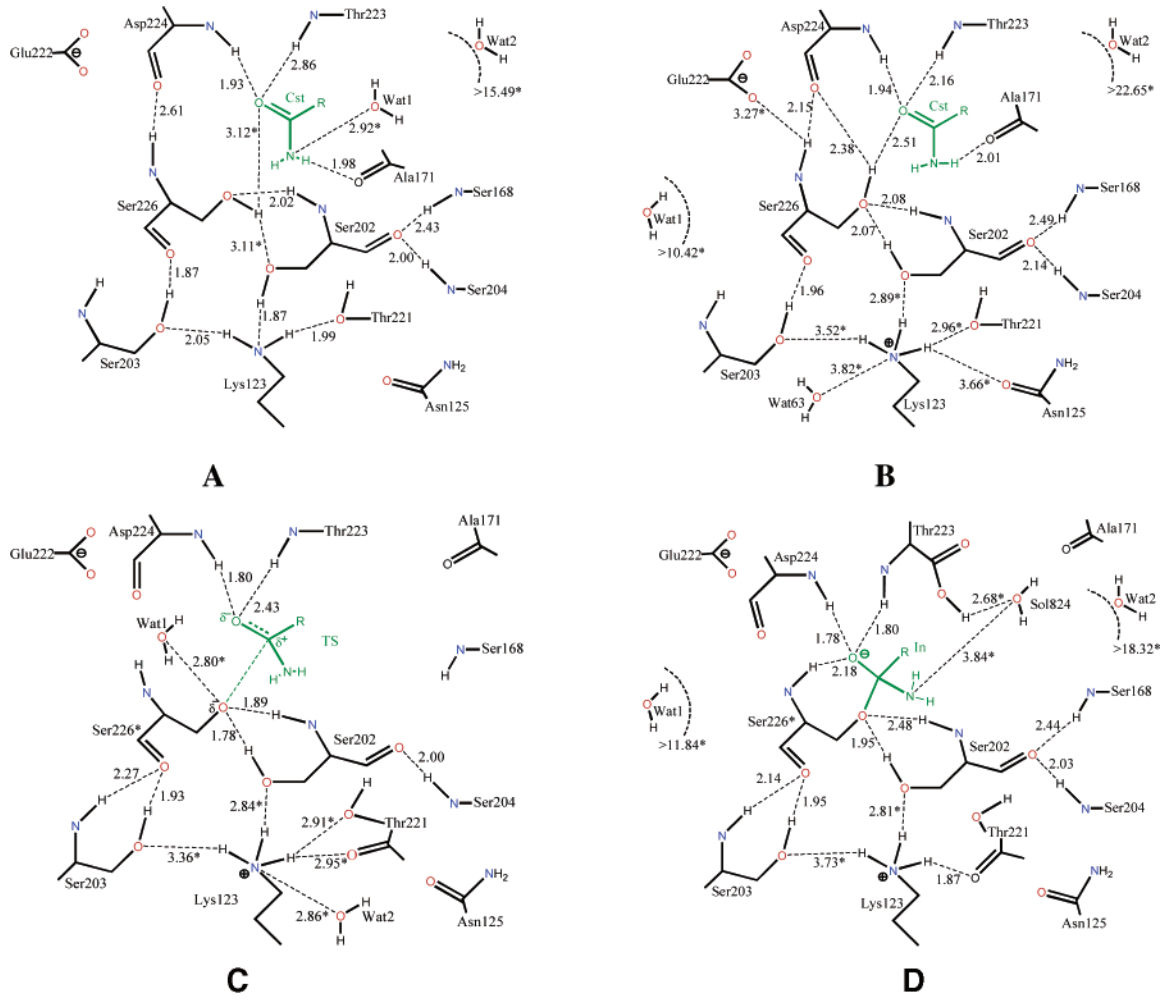

[a] All distances are in angstroms. The substrate is colored green. Asterisks indicate distances between heavy atoms.

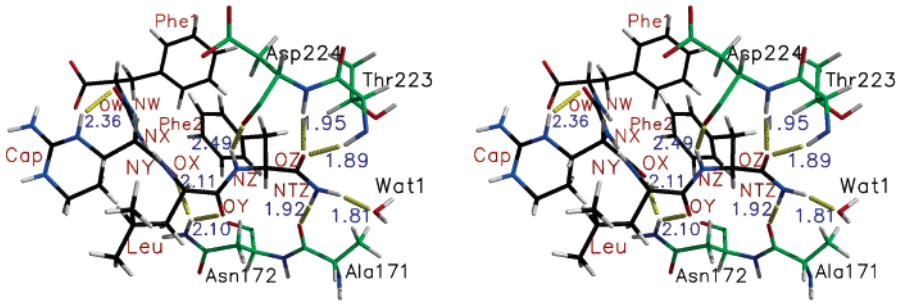

FIGURE 5: Stereoview of the average structure of the MD simulation of the E·S system showing hydrogen bonding interactions with Cst-NH_2. Distances between the electronegative atom and the hydrogen atom are given in angstroms. The carbon atoms of the substrate are shown in black.

is hydrogen bonded with both the carbonyl oxygens, OY ($R_{OY\cdots H}$ = 2.88 ± 0.45 Å) and OX ($R_{OX\cdots H}$ = 2.18 ± 0.25 Å), of Cst-NH_2. The backbone amide oxygen of Asp224 is mobile, making infrequent hydrogen bonds with the amide nitrogen (NZ) of Cst-NH_2 ($R_{O\cdots N}$ = 3.78 ± 0.33 Å). With regard to the crystallographic waters, Wat1 is hydrogen bonded to NZ of Cst-NH_2 ($R_{O\cdots NZ}$ = 2.96 ± 0.17 Å), whereas Wat2 moves out from the active site ($R_{O\cdots NZ}$ = 22.72 ± 2.9 Å). Often in MD simulation, the water of crystallization has been shown to be mobile, and in some cases, it is exchanged with other water molecules from the solvent (*24*). The position of these waters in the X-ray crystal structure is shown in Figure 1. The intramolecular hydrogen bonding between the amide oxygen (OW) and the amine hydrogen of the Cap ring of Cst-NH_2 might assist in directing the polar portion of the Cap ring toward the solvent surrounding.

Nonpolar Interactions within the Active Site of the E·S System. Residues that are within van der Waals distance of Cst-NH_2 in the E·S system are shown in Figure 6. The bulky alkyl groups of Leu407, Leu363, and the benzene ring of Phe173 make hydrophobic contacts with Phe rings of Cst-NH_2 with heavy atom distances of 3.95 ± 0.26, 4.02 ± 0.41, and 3.71 ± 0.22 Å, respectively. The nonpolar $(CH_2)_n$ chain of Arg360 is 4.00 ± 0.34 Å from the Phe1 ring of the

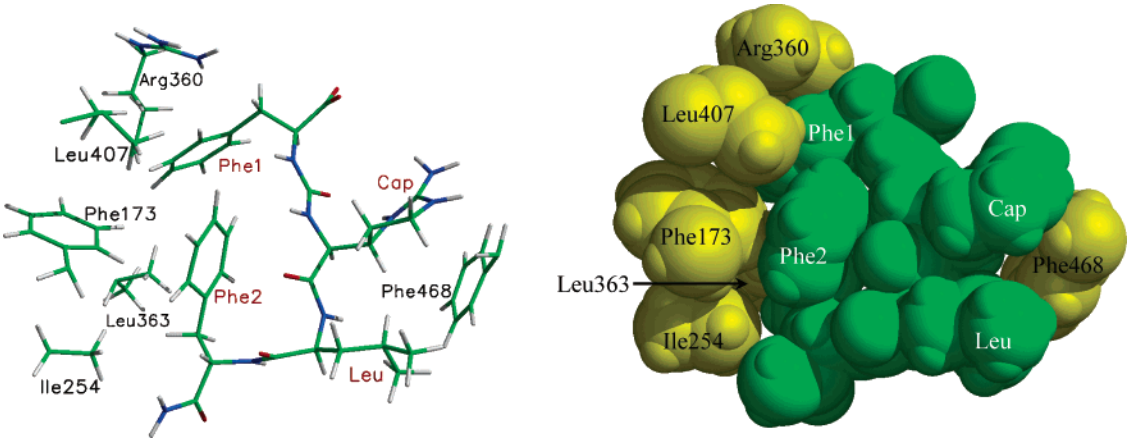

FIGURE 6: Average structure of the MD simulation of the E·S system showing hydrophobic interactions between the substrate Cst-NH_2 and the active site. Cst-NH_2 is colored green (with red labels), and the nearby residues are colored yellow (with black labels). Parts of the substrate are labeled red and white.

substrate. Ile254 is within hydrophobic contact distance of the Phe2 ring of the substrate (3.98 ± 0.25 Å). The benzene ring of Phe468 interacts with the hydrophobic part of the Cap ring (4.39 ± 0.38 Å) and the Leu chain (4.22 ± 0.68 Å) of Cst-NH_2.

MD Simulations of the EH·S Ground State (with Lys123-NH_3^+)

Polar Interactions within the Active Site of the EH·S System. Chart 3B displays the hydrogen bonding interactions with the reactive amide group of Cst-NH_2 and the catalytic residues within the active site. The nucleophilic hydroxyl oxygen of Ser226-OH remains close (3.37 ± 0.20 Å) to the electrophilic carbonyl carbon atom of Cst-NH_2, while stable hydrogen bonding interactions are observed among Ser-Ser-Lys catalytic residues.

During the simulation, the amide hydrogens of Thr223 and Asp224 make strong and prominent hydrogen bonds with the terminal carbonyl oxygen of Cst-NH_2, with the following distances: $R_{O\cdots H}$ = 2.16 ± 0.21 Å and $R_{O\cdots H}$ = 1.94 ± 0.15 Å, respectively. The position of the hydrogen of Ser226-OH changes direction to make three different hydrogen bonds during the 16 ns simulation (Figure 7). Initially, the hydrogen of Ser226-OH is hydrogen bonded to the terminal amide oxygen of Cst-NH_2 ($R_{O\cdots O}$ = 3.12 ± 0.24 Å and $R_{O\cdots H}$ = 2.51 ± 0.38 Å). After the initial 1 ns of the simulation time, the position of the hydrogen of Ser226-OH begins to fluctuate in hydrogen bonding between the substrate's amide oxygen (C=ONH_2) and the amide carbonyl oxygen of Asp224 ($R_{O\cdots H}$ = 2.38 ± 0.40 Å). As the MD simulations progress, the hydrogen of Ser226-OH becomes more strongly hydrogen bonded with the backbone oxygen of Asp224. After 10 ns, there is a rare occurrence of hydrogen bonding between the hydrogen of Ser226-OH and oxygen of Ser202-OH (red lines in Figure 7C), causing the hydrogen of Ser202-OH to point away from the hydroxyl group of Ser226-OH haphazardly with a hydrogen-bonded conformer population of less than 1% of the observation time. Ser202 continues to interact with Ser226 through a stronger and stable hydrogen bond between the hydrogen of Ser202-OH and the hydroxyl oxygen of Ser226-OH (green lines in Figure 7C) with a heavy atom distance of 2.86 ± 0.16 Å ($R_{O\cdots H}$ = 2.07 ± 0.42 Å), and a weaker hydrogen bond between the amide hydrogen of Ser202 and the hydroxyl oxygen of Ser226-OH with a heavy atom distance of 3.03 ± 0.16 Å ($R_{O\cdots H}$ = 2.08 ± 0.17 Å). Throughout the EH·S simulation, hydrogen bonding between Lys123-NH_3^+ and the hydroxyl oxygen of Ser202-OH prevails ($R_{O\cdots N}$ = 2.89 ± 0.16 Å).

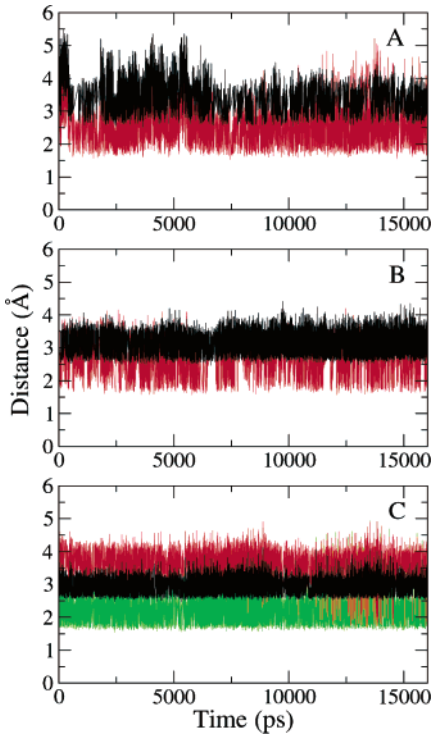

FIGURE 7: Histogram for the EH·S system showing hydrogen bond distances in angstroms between (A) the hydroxyl oxygen of Ser226-OH and the amide oxygen of Ser224, (B) the hydroxyl oxygen of Ser226-OH and the terminal amide oxygen of Cst-NH_2, and (C) the hydroxyl oxygen of Ser226-OH and the hydroxyl oxygen of Ser202-OH. The black lines represent heavy atom distances. Red lines represent distances between an electronegative atom and the hydroxyl hydrogen of Ser226-OH. Green lines represent the distance between the hydroxyl oxygen of Ser226-OH and the hydroxyl hydrogen of Ser202-OH.

Strong hydrogen bonds occur between the amine hydrogens of Lys123-NH_3^+ and hydroxyl oxygens of Ser203-OH and Thr221-OH, with heavy atom distances of the former being 3.52 ± 0.56 Å and the latter 2.96 ± 0.21 Å. After 360 ps, the side chain amide oxygen of Asn125 migrates to hydrogen bond with the amine hydrogens of Lys123-NH_3^+

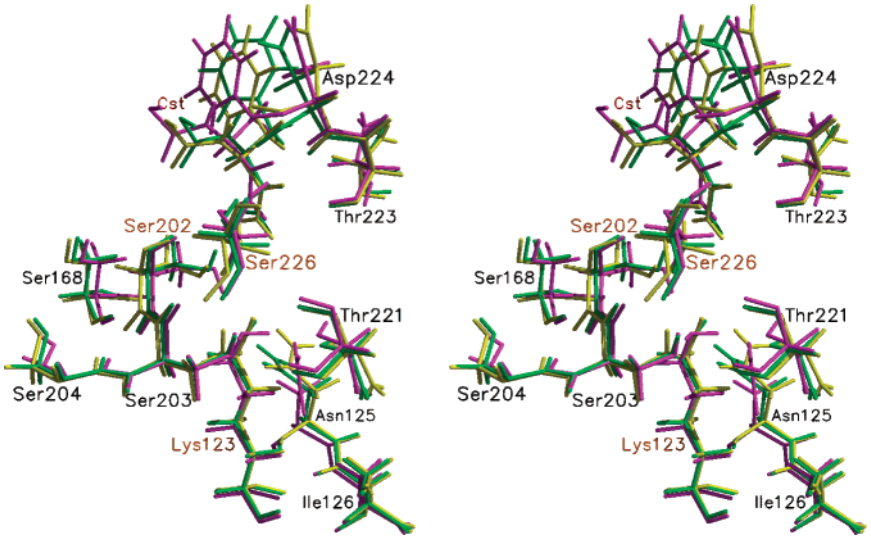

FIGURE 8: Superposition of the average structures from MD simulations of the E·S system (magenta), the EH·S system (green), and the E⁻H·S system (yellow). Important residues that are hydrogen bonded to the catalytic residues and Cst-NH_2 within the active site are shown. The catalytic triad residues are colored orange.

($R_{O\cdots N}$ = 3.66 ± 0.60 Å). This hydrogen bonding is not observed in the E·S model.

In a comparison of the amide hydrogen bonding to the carbonyl oxygen of Ser202 by Ser168 ($R_{O\cdots N}$ = 3.37 ± 0.26 Å) and Ser204 ($R_{O\cdots N}$ = 2.99 ± 0.15 Å), the latter predominates. The hydroxyl oxygen of Ser203-OH is strongly hydrogen bonded to the backbone oxygen of Ser226 ($R_{O\cdots O}$ = 2.84 ± 0.18 Å and $R_{O\cdots H}$ = 2.00 ± 0.24 Å). After 400 ps, the amide oxygen of Asp224 moves closer and hydrogen bonds to the amide hydrogen of Ser226 ($R_{O\cdots N}$ = 2.84 ± 0.15 Å). During the EH·S dynamics, the carboxylate Glu222-CO_2^- is infrequently hydrogen bonded to the amide hydrogen of Ser226 ($R_{O\cdots N}$ = 3.27 ± 0.25 Å).

The direct hydrogen bonding interactions with Cst-NH_2 in the EH·S system are similar to those of the E·S system as shown in Figure 5. There persists a hydrogen bond between the backbone amide oxygen of Ala171 and the terminal amide nitrogen of Cst-NH_2 ($R_{O\cdots H}$ = 2.01 ± 0.20 Å). Both the carbonyl amides OY ($R_{OY\cdots H}$ = 2.74 ± 0.68 Å) and OX ($R_{OY\cdots H}$ = 2.63 ± 0.68 Å) of Cst-NH_2 interact weakly with the amide hydrogen of Asn172. The amide nitrogen (NZ) of Cst-NH_2 makes frequent contact with the backbone oxygen of Asp224 ($R_{O\cdots N}$ = 2.85 ± 0.39 Å). Both the crystallographic waters, Wat1 and Wat2, move out from the active site ($R_{O\cdots NZ}$ > 20 Å), but another crystallographic water (Wat163) replaces Wat1 and occasionally hydrogen bonds with NZ of Cst-NH_2 ($R_{O\cdots N}$ = 5.00 ± 1.57 Å). The amide NY of the substrate makes intermittent weak contact with the carboxyl group of Asp224-COO^- ($R_{N\cdots O}$ = 3.43 ± 0.76 Å). A hydrogen bond between the amide OW and the amine hydrogen (Cap ring) within Cst-NH_2 is maintained, directing the polar group of the Cap ring toward the water environment.

Nonpolar Interactions within the Active Site of the EH·S System. The nonpolar interactions observed in EH·S are much the same as in E·S (Figure 6). Leu407 makes indirect contact with both Phe1 (3.89 ± 0.29 Å) and Phe2 (4.30 ± 0.65 Å) rings of Cst-NH_2. Phe173 also forms a hydrophobic interaction with the Phe1 (4.24 ± 0.51 Å) and Phe2 (4.62 ± 0.95 Å) rings of the substrate. Leu363 is 4.01 ± 0.35 Å from the Phe1 ring. In addition, the Phe1 ring is held within the active site by a hydrophobic contact with the nonpolar alkyl chain of Arg360 (4.12 ± 0.46 Å) and the Phe2 ring via contact with Ile254 (4.07 ± 0.53 Å). The Cap ring of Cst-NH_2 is solvent-exposed, while its nonpolar part makes hydrophobic contact with the benzene ring of Phe468 (3.93 ± 0.42 Å). Leu of the substrate is 4.86 ± 0.74 Å from Phe468.

MD Simulations of the E−H·S Ground State (with Ser226-O− and Lys123-NH_3^+)

Polar Interactions within the Active Site of the E⁻H·S System. During the 2 ns MD simulation of the E⁻H·S system, a hydrogen bonding network exists among the catalytic residues in which Lys123-NH_3^+ is hydrogen bonded to the hydroxyl oxygen of Ser202-OH and the hydroxyl hydrogen of Ser202-OH is hydrogen bonded to the deprotonated hydroxyl oxygen of Ser226-O^- (with heavy atom average distances of 2.89 ± 0.13 and 2.69 ± 0.09 Å, respectively). Both the amide hydrogen of Thr223 and that of Asp224 interact with the amide carbonyl oxygen of the substrate. Even though the average production dynamics for the E⁻H·S system can be superimposed with the ground state E·S and EH·S systems (Figure 8), nucleophilic Ser226-O^- in the E⁻H·S system does not remain within van der Waals distance (∼3.33 Å) of the electrophilic carbonyl carbon of Cst-NH_2. After the initial constraint between the hydroxyl oxygen of Ser226-O^- and the amide carbonyl carbon of Cst-NH_2 has been removed, Ser226-O^- moves away from the carbonyl carbon of Cst-NH_2 at an initial heavy atom distance of ∼3.20−4.20 Å. At this distance, the reaction between Ser226-O^- and the electrophilic carbonyl carbon is highly unlikely. Thus, further investigation of this system was discontinued.

MD Simulations of the E·TS Transition State

Polar Interactions within the Active Site of the E·TS System. During the 10 ns simulation of E·TS, a hydrogen bonding network prevails among the catalytic residues displayed in Figure 9. The hydroxyl oxygen and amide nitrogen of Ser202-OH make strong contacts with the hydroxyl oxygen (OG_{TS}) of Ser226*, now a part of TS, with

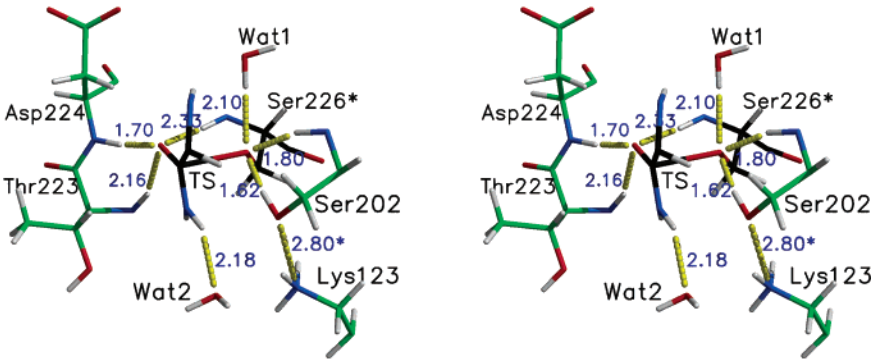

FIGURE 9: Stereoview of a snapshot from the E·TS system, formed from E·S, MD simulation (nearing 6 ns) showing the hydrogen bonding distances in angstroms between the heavy atom and hydrogen atom. Ser226* represents Ser226 as part of the transition state (TS). Asterisks indicate distances between heavy atoms.

heavy atom distances of 2.73 ± 0.09 ($R_{O\cdots H}$ = 1.78 ± 0.09 Å) and 2.87 ± 0.10 Å ($R_{O\cdots H}$ = 1.89 ± 0.10 Å), respectively. Lys123-NH_3^+ makes a stable hydrogen bond with Ser202 ($R_{N\cdots O}$ = 2.84 ± 0.12 Å). Both the amide hydrogen of Thr223 and that of Asp224 continue to interact with the increased negative charge on the amide oxygen of TS, where the Thr223 hydrogen bond is the weaker ($R_{O\cdots H}$ = 2.43 ± 0.19 Å) that that of Asp224 ($R_{O\cdots H}$ = 1.80 ± 0.10 Å).

Chart 3C displays the residues within the active site that hydrogen bond to the TS and position the catalytic residues for catalysis. The amide nitrogen of Ser204 maintains close contact with the carbonyl oxygen of Ser202 ($R_{N\cdots O}$ = 2.86 ± 0.12 Å), while the amide nitrogen of Ser168 moves away from Ser202 (>5 Å) after 2 ns of simulation time. The amino protons of Lys123-NH_3^+ interact weakly with Ser203-OH ($R_{N\cdots O}$ = 3.36 ± 0.34 Å) and strongly with Thr221-OH ($R_{N\cdots O}$ = 2.91 ± 0.15 Å). In addition, Lys123-NH_3^+ interacts with the amide oxygen of Thr221 ($R_{N\cdots O}$ = 2.95 ± 0.18 Å). In comparison to the dynamics of the E·S system, the amide nitrogen of Ser226* in the E·TS model does not hydrogen bond to the carbonyl oxygen of Asp224. Instead, the amide hydrogen of Ser226* is hydrogen bonded to the terminal amide oxygen of the TS only for the first 3.0 ns before E·TS reaches equilibrium at 4 ns (Figure 2C). After 2.5 ns of simulation time, the backbone nitrogen of Ser203-OH joins with the hydroxyl oxygen of Ser-OH to hydrogen bond to the backbone amide oxygen of Ser226*, with the following heavy atom distances: $R_{O\cdots O}$ = 3.16 ± 0.19 Å and $R_{O\cdots O}$ = 2.80 ± 0.14 Å, respectively.

In the E·TS system, the residues involved in hydrogen bonding to the TS are similar to the residues in E·S as shown in Figure 5, with the exception of Ala171. Ala171 does not associate with the terminal amide NH_2 group of the TS as observed in the ground states (E·S and EH·S). Crystallographic water Wat1 closely interacts with OG_{TS} of Ser226* ($R_{O\cdots O}$ = 2.89 ± 0.10 Å), and Wat2 interacts with the terminal amide NH_2 group of the TS ($R_{O\cdots NZ}$ = 3.40 ± 0.31 Å). Wat1 is hydrogen bonded to a solvent water molecule, Sol138 ($R_{O\cdots O}$ = 2.90 ± 0.11 Å), which in turn is hydrogen bonded to Asp224 ($R_{O\cdots O}$ = 2.72 ± 0.11 Å) and Tyr473 ($R_{O\cdots O}$ = 2.92 ± 0.2 Å). While the backbone nitrogen of Asp224 maintains close contact with the terminal carbonyl oxygen of the TS, the carboxylic group of Asp224-COO^- moves closer and becomes strongly hydrogen bonded to the amide nitrogen (NY) of the TS ($R_{O\cdots H}$ = 1.86 ± 0.15 Å) after the initial 1.5 ns of the MD simulation. The side chain hydrogen of Asn172-C=ONH_2 interacts with the amide oxygen (OX) of the TS occasionally ($R_{O\cdots H}$ = 3.13 ± 0.79 Å). Throughout the E·TS simulation, the amide oxygen (OW) and the amine nitrogen of the Cap ring of the TS make weak contact with each other ($R_{O\cdots H}$ = 2.78 ± 0.50 Å).

Nonpolar Interactions within the Active Site of the E·TS System. The residues shown in Figure 6 for E·S continue to interact with the hydrophobic part of the TS. Phe173 forms a stronger interaction with the Phe rings of TS ($R_{C\cdots C}$ = 3.54 ± 0.26 Å and $R_{C\cdots C}$ = 3.57 ± 0.26 Å), pushing Leu407 to form an interaction with only the Phe1 ring of the TS ($R_{C\cdots C}$ = 4.61 ± 0.64 Å). The $(CH_2)_n$ groups of Arg360 and Leu363 continue to interact with the Phe1 ring within the active site, with van der Waals contact distances of 3.69 ± 0.28 and 3.97 ± 0.55 Å, respectively. Ile254 and Leu363 make weaker contacts with the Phe2 ring with contact distances of 4.01 ± 0.25 and 4.59 ± 0.49 Å, respectively. The methylene of Thr223 is closer to the Phe2 ring ($R_{C\cdots C}$ = 4.01 ± 0.25 Å), keeping the amide NH group of Thr223 in good position to hydrogen bond with OZ of the TS. Ala171 seems to be more stable interacting with the Leu part of the TS, with an average van der Waals distance of 4.58 Å. Phe468 continues to make hydrophobic contact with the Cap ring and the Leu part of the TS, with distances of 3.76 ± 0.29 and 4.16 ± 0.44 Å, respectively.

MD Simulations of the E·In Tetrahedral Intermediate State

Polar Interactions within the Active Site of the E·In System. The hydrogen bonding interactions for the E·In system are shown in Chart 3D. During the 10 ns simulation, Lys123 is strongly hydrogen bonded to Ser202 with a heavy atom distance of 2.81 ± 0.11 Å, while the bridging residue, Ser202, makes three contacts with the tetrahedral intermediate (In) (refer to Figure 10). Ser202-OH maintains its hydrogen bonding to the hydroxyl oxygen of Ser226*, with a heavy atom distance of 2.80 ± 0.11 Å ($R_{O\cdots H}$ = 1.95 ± 0.17 Å). With the weaker and intermittent contact made by the backbone nitrogen of Ser202 with the hydroxyl oxygen of Ser226* ($R_{O\cdots N}$ = 3.41 ± 0.19 Å), Ser202 is more flexible and able to move closer and make good contact with the terminal amide NH_2 group of the intermediate ($R_{O\cdots N}$ = 3.30 ± 0.24 Å) during the simulation (Figures 10 and 11B). However, after ~4 ns of the E·In simulation, the amino group of Lys123-NH_3^+ also establishes a hydrogen bond with the NH_2 substituent of the tetrahedral intermediate with a heavy

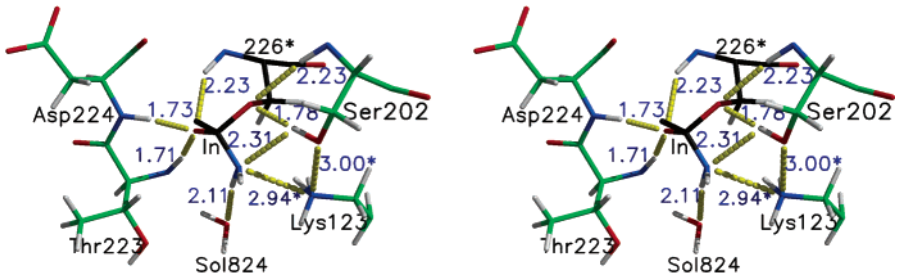

FIGURE 10: Stereoview of a snapshot from the E·In system MD simulation (nearing 8 ns) showing the hydrogen bonding distances in angstroms between the heavy atom and the hydrogen atom. Ser226* represents Ser226 as part of the intermediate (In). Asterisks indicate distances between heavy atoms.

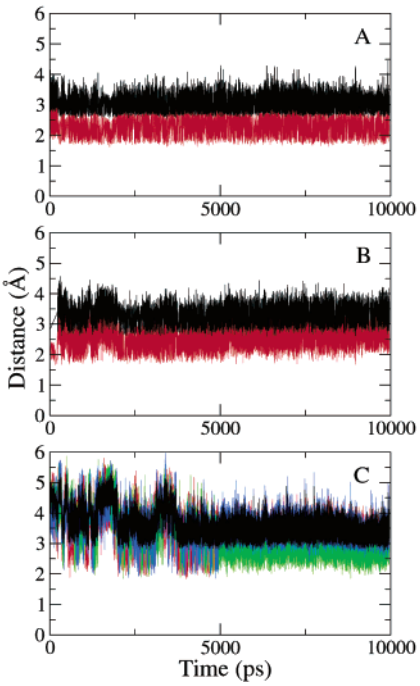

FIGURE 11: Histogram for the E·In system showing hydrogen bond distances in angstroms between (A) the amide nitrogen of Ser226*, now part of the tetrahedral intermediate, and the negatively charged oxygen of the tetrahedral intermediate (In), (B) the terminal amide NH_2 group of In and the hydroxyl oxygen of Ser202-OH, and (C) the amide NH_2 group of In and the amino group of Lys123-NH_3^+. The black lines represent heavy atoms distances. The lines colored red, blue, and green represent the distances between an electronegative atom and a hydrogen atom.

atom distance of 3.43 ± 0.26 Å as shown in Figures 10 and 11C. The negative charge on the oxyanion of the intermediate is stabilized by strong hydrogen bond contacts with the amide hydrogen of Asp224 ($R_{O\cdots H}$ = 1.78 ± 0.11 Å) and Thr223 ($R_{O\cdots H}$ = 1.80 ± 0.10 Å). From the trajectory (Figure 11A), the amide nitrogen of Ser226* is now hydrogen bonded to the negatively charged oxygen of the intermediate ($R_{O\cdots H}$ = 2.19 ± 0.23 Å).

As displayed in Chart 3D, the backbone nitrogen of Ser204 remains in contact with the carbonyl oxygen of Ser202 ($R_{N\cdots O}$ = 2.89 ± 0.12 Å) while the amide nitrogen of Ser168 makes weak and occasional contact with the carbonyl oxygen of Ser202 ($R_{N\cdots O}$ = 3.33 ± 0.23 Å). The conserved residues in AS enzymes, Ser203 and Thr221, continue to interact with Lys123. A weak contact is observed between the amino group of Lys123-NH_3^+ and Ser203-OH ($R_{N\cdots O}$ = 3.73 ± 0.28 Å). Even though the hydroxyl group of Thr221-OH loses interaction with Lys123-NH_3^+ before the rmsd equilibrium was reached at 6 ns (Figure 2D), the hydrogen bond between Lys123-NH_3^+ and the amide oxygen of Thr221 becomes even more prominent ($R_{N\cdots O}$ = 2.84 ± 0.13 Å).

The residues in contact in E·S (Figure 5) make direct contact with the tetrahedral intermediate. The amide oxygen of Asp224 is held close to stabilize the oxyanion species by making contact with the backbone nitrogen (NZ) ($R_{O\cdots N}$ = 2.86 ± 0.13 Å) and weakly and rarely with the amide nitrogen (NY) of the intermediate ($R_{O\cdots N}$ = 3.22 ± 0.20 Å). However, the carboxylate of Asp224-COO^- does not contact In. Meanwhile, Ser203-OH makes a stronger hydrogen bond contact with the amide oxygen of Ser226* ($R_{O\cdots O}$ = 2.82 ± 0.15 Å) in comparison to the contact made by the backbone nitrogen of Ser203 with the amide oxygen of Ser226* ($R_{N\cdots O}$ = 3.04 ± 0.16 Å). The side chain amide nitrogen of Asn172-C═ONH_2 barely interacts with the amide oxygen (OY) ($R_{N\cdots O}$ = 3.72 ± 0.38 Å) and OX of the intermediate ($R_{N\cdots O}$ = 3.36 ± 0.36 Å). During the 10 ns trajectory, the amide oxygen (OW) and the amine nitrogen of the Cap ring make weak contact with each other ($R_{O\cdots H}$ = 2.61 ± 0.32 Å) which might expose the polar part of the Cap ring to the solvent.

Nonpolar Interactions within the Active Site of the E·In System. The hydrophobic interactions are weaker in E·In than in E·S (Figure 6). Leu363 interacts with both Phe rings of the intermediate ($R_{C\cdots C}$ = 4.44 ± 0.55 and 4.46 ± 0.46 Å), while Phe173 interacts more closely with the Phe2 ring ($R_{C\cdots C}$ = 3.87 ± 0.33 Å) than with the Phe1 ring ($R_{C\cdots C}$ = 4.14 ± 0.68 Å) to keep the active part of the intermediate intact and allows Leu407 to make good contact with the Phe1 ring ($R_{C\cdots C}$ = 4.43 ± 0.83 Å). The $(CH_2)_n$ group of Arg360 remains in contact with the Phe1 ring ($R_{C\cdots C}$ = 4.62 ± 0.81 Å). Both Ile254 and the alkyl group of Thr223 interact with the Phe2 ring, with van der Waals distances of 4.85 ± 0.41 and 4.54 ± 0.26 Å, respectively. Phe468 remains within hydrophobic contact distance of the Cap ring ($R_{C\cdots C}$ = 4.46 ± 0.84 Å) and the Leu part of the intermediate ($R_{C\cdots C}$ = 4.11 ± 0.47 Å). Ala171 does not make any contact with the intermediate.

DISCUSSION

Long-term MD simulations were carried out for the five systems (E·S, EH·S, E^-H·S, E·TS, and E·In) shown in Chart 1 in an effort to investigate the possible steps of the Ser-Ser-Lys catalytic triad mechanism for hydrolysis of the peptide by Pam. The segment of residues 464−466 is significantly different in the native and inhibitor-bound structure of Pam (*9*). This segment, however, can be superimposed on the average structure obtained from MD

Table 1: Comparison of Hydrogen Bonding Distances (Angstroms) to the Substrate (Cst-NH_2) and to the Catalytic Residues from X-ray (PDB entry 1M21), EH·S, and E·S Systems

	X-ray	EH·S	E·S
Cst-NH_2(CZ)−Ser226(OG)	2.51	3.37 ± 0.20	3.18 ± 0.17
Cst-NH_2(CZ)−Ser202(OG)	3.02	4.01 ± 0.22	4.21 ± 0.20
Cst-NH_2(OZ)−Ser226(OG)	2.90	3.12 ± 0.24	3.12 ± 0.30
Cst-NH_2(OZ)−Ser202(OG)	2.92	4.36 ± 0.25	4.75 ± 0.25
Cst-NH_2(OZ)−Asp224(N)	5.13	2.91 ± 0.14	2.92 ± 0.17
Cst-NH_2(OZ)−Thr223(N)	4.27	3.05 ± 0.17	3.71 ± 0.31
Cst-NH_2(NTZ)−Ala171(O)	*a*	2.97 ± 0.18	2.93 ± 0.16
Cst-NH_2(NTZ)−Ser202(OG)	*a*	3.33 ± 0.25	3.18 ± 0.19
Cst-NH_2(OX)−Asn172(ND2)	2.92	3.29 ± 0.62	2.97 ± 0.17
Cst-NH_2(OY)−Asn172(ND2)	3.15	3.39 ± 0.47	3.51 ± 0.35
Ser226(OG)−Ser202(OG)	2.53	2.73 ± 0.09	3.11 ± 0.25
Ser226(OG)−Ser202(N)	3.15	2.87 ± 0.10	2.99 ± 0.15
Ser202(OG)−Lys123(NZ)	2.81	2.84 ± 0.11	2.79 ± 0.09

[a] The X-ray structure of Pam in complex with Cst does not have the terminal amide nitrogen group (NH_2).

simulations of E·S, EH·S, E^-H·S, and E·TS. The dynamics of the ground states, E·S and EH·S, were compared to determine the favored protonation state of Lys123 during the nucleophilic addition of the hydroxyl oxygen of Ser226-OH to the amide carbonyl function of the substrate. The E^-H·S ground state differs from E·S and EH·S by having a deprotonated nucleophile (Ser226-O^-). The geometrical prerequisites for the formation of the transition state (TS) and, in turn, the tetrahedral intermediate (In) were investigated to identify the catalytically competent ground state of the three plausible ground states. E·TS and E·In were studied to determine the stability of the tetrahedral oxyanion intermediate within the active site. The MD trajectory of the E·In system was also analyzed to study the collapse of the tetrahedral intermediate and formation of the acyl−enzyme product.

Comparison of the E·S, EH·S, and E−H·S Ground States

The average structures from MD simulations of the E·S (with Lys123-NH_2) and EH·S (with Lys123-NH_3^+) ground states can be superimposed on each other and on the E^-H·S system as shown in Figure 8. Comparisons of the distance of the catalytic residues and the substrate from the X-ray structure of Pam, and the MD structures of EH·S and E·S systems, are shown in Table 1. The Cst-NH_2(OZ)−Asp224-(N) and Cst-NH_2(OZ)−Thr223(N) distances show a large deviation (>1.2 Å) from the X-ray crystal structure. This is not very surprising because the substrate that is modeled in the MD simulation presents to the active site with the −C(═O)NH_2 group terminal while the substituent in the X-ray structure is the −C(═O)H group. In the X-ray crystal structure (Figure 1), Wat1 is hydrogen bonded to Asp224 and Thr223 backbone amide hydrogens, but in our MD simulations, Asp224 and Thr223 backbone amides hydrogen bond (forming an oxyanion hole) directly to the amide carbonyl of Cst-NH_2 (Chart 3). Hence, a difference from the X-ray structure is observed. The direct interaction of the amide carbonyl of Cst-NH_2 with the oxyanion hole is justified due to the increased polarity of the amide oxygen in Cst-NH_2 compared to the carbonyl oxygen in Cst. Also, Cst occupies a smaller molar volume than Cst-NH_2, and hence, the vacant space in the X-ray is filled up by crystallographic waters. For instance, the X-ray structure of chymotrypsin has crystallographic waters interacting with the oxyanion hole in the absence of a substrate (*25*).

The MD simulations for the E·S and EH·S ground states agree with the previous proposal that Ser226-OH (*9*) is the only catalytic triad residue that makes contact with the substrate. *cis*-Ser202 bridges the hydroxyl oxygen of Ser226 and the amine group of Lys123. In both E·S and EH·S systems, the backbone amide NH groups of Asp224 and Thr223 are within hydrogen bonding distance of the carbonyl amide oxygen of the substrate to assist the nucleophilic addition reaction.

We use geometrical criteria based on the reactive Michaelis complex to compare the three ground states (E·S, EH·S, and E^-H·S). The two parameters that we use to define the reactive Michaelis complex species for the formation of the acyl−enzyme intermediate are the van der Waals contact distance of ≤3.33 Å and an approaching angle of 113 ± 20° between the nucleophilic hydroxyl oxygen of the nucleophilic Ser226 and the electrophilic amide carbonyl carbon of the substrate. We term these reactive ground state species NACs. The criteria for NAC formation are used to determine the population of the reactive Michaelis complex in all three ground states. The percentage of time the Michaelis conformer exists as a NAC is 68.3% in E·S (Figure 3A), which is ∼2-fold (31.0%) greater than that in EH·S (Figure 3B). On the basis of the steric criteria, E^-H·S would be omitted as a potential ground state for the Pam enzyme as this system forms a very small population (0.1%) of reactive species. On the other hand, the Ser226-O^- alkoxide is a better nucleophile than Ser226-OH. This is offset by the unlikely existence of Ser226-O^- at neutral pH.

Examination of panels A and B of Figure 12 suggests that the hydrogen bonding configuration of the E·S system both provides a direct route for activation of the nucleophilic Ser226-OH and maintains the van der Waals contact with the electrophilic carbonyl carbon of the substrate, and thus, the E·S complex with Lys-NH_2 provides a more compelling model. However, the percentage of time the Michaelis complex exists as NACs in E·S or EH·S is rather comparable (Figure 3), suggesting two competitive mechanisms.

The experimental rate constants (*26*) as a function of pH (Figure 13) support one rate-determining process at a lower pH and a second rate-determining process at a somewhat higher pH. Further, both mechanisms are characterized by bell-shaped pH profiles. Hence, the kinetic Scheme 2 is suggested. Scheme 2 is derived using the assumption that the formation of the acyl−enzyme intermediate is the rate-determining step. At a lower pH, the Michaelis species of importance are M1, M2, and M3 (M_T). At a higher pH, theMichaelis species of importance are M2, M3, and M4 (M'_T). As a result, at low pH (*27*)

$$v_1 = k_1[\mathrm{M2}] = k_1[\mathrm{M_T}]\left(\frac{Ka_1a_\mathrm{H}}{a_\mathrm{H}^2 + Ka_1a_\mathrm{H} + Ka_1Ka_2}\right)$$

And, at high pH

$$v_2 = k_2[\mathrm{M3}] = k_2[\mathrm{M'_T}]\left(\frac{Ka_2a_\mathrm{H}}{a_\mathrm{H}^2 + Ka_2a_\mathrm{H} + Ka_2Ka_3}\right)$$

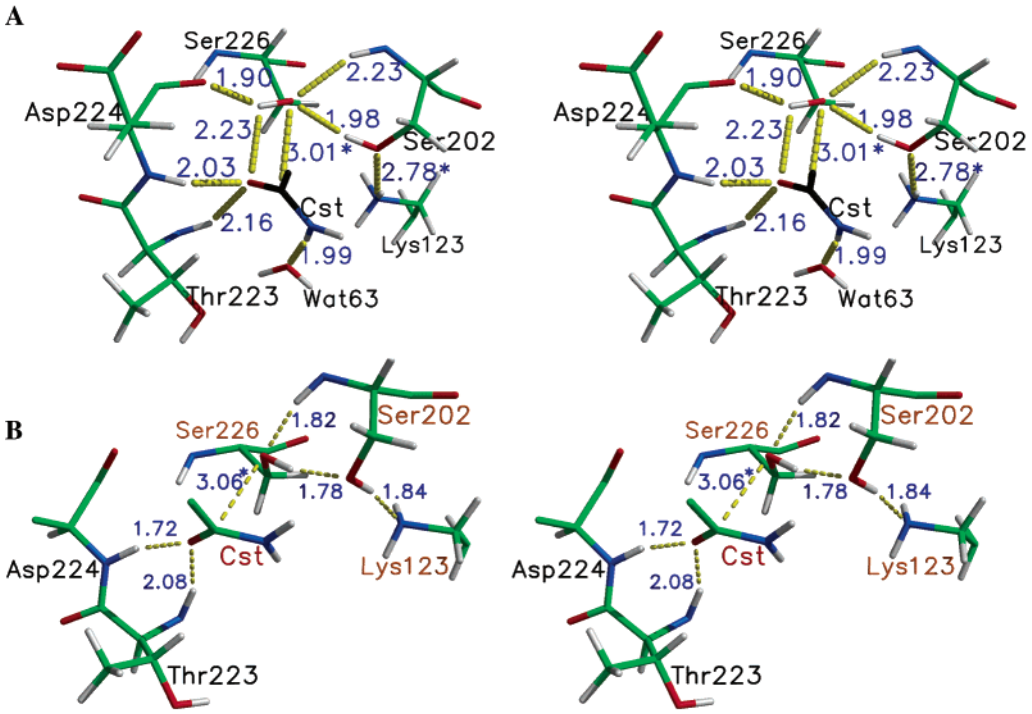

FIGURE 12: Stereoview of a snapshot from the EH·S (A) and E·S (B) system MD simulation (nearing 12 ns) showing the hydrogen bonding distances in angstroms between the heavy atom and the hydrogen atom. The heavy atom distance between the nucleophilic hydroxyl oxygen of Ser226-OH and the amide carbonyl carbon atom of Cst-NH_2 is also shown. The catalytic triad residues are labeled in orange. Asterisks indicate distances between heavy atoms.

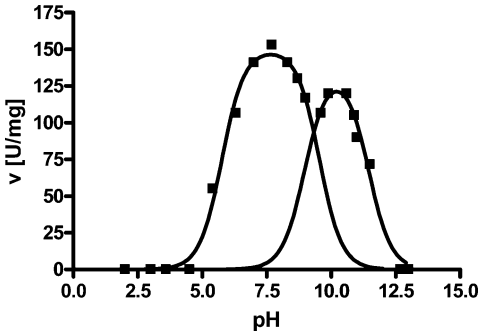

FIGURE 13: Plot of the experimental pH−rate profile (*26*) for the hydrolysis of Ala-Phe-NH_2 by Pam. The pH−rate profile refers to the overall reaction, the production of ammonia. The lines fitted to the experimental points have been derived from eq 1 based upon Scheme 2. The pH−rate profile shows two bell-shaped curves which supports two competitive, pH-dependent mechanisms. The fitting procedure was performed using GraphPad Prism version 4.00 for Windows (GraphPad Software, San Diego, CA).

Scheme 2

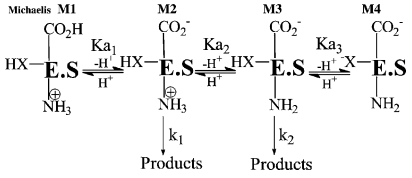

Therefore, the overall rate equation can be written as

$$v_1 = k_1[\mathrm{M_T}]\left(\frac{Ka_1a_\mathrm{H}}{a_\mathrm{H}^2 + Ka_1a_\mathrm{H} + Ka_1Ka_2}\right) + k_2[\mathrm{M'_T}]\left(\frac{Ka_2a_\mathrm{H}}{a_\mathrm{H}^2 + Ka_2a_\mathrm{H} + Ka_2Ka_3}\right) \quad (1)$$

Examination of Figure 13 establishes that the "double-bell" pH profile is fit by eq 1 (correlation coefficient = 0.99) when k_1 and k_2 equal 140.7 and 126.8 s^{-1}, respectively, and the pK_{app} values are 5.8, 9.1, 9.5, and 11.4. The pK_{app} values of 9.1 and 9.5 are only 0.4 unit apart and are reasonable for the ionization of Lys110-NH_3^+. The pK_{app} of 5.8 may correspond to the enzymatic carboxylate group (Asp224) or the terminal carboxylate of the substrate. Asp224 plays an important role in the proton relay via the structured water channel (*vide infra*). The pK_{app} of 11.4 may correspond to Arg360 that is within 4.5 Å of the terminal carboxyl of the substrate. The pK_{app} of 11.4 may also be considered to be due to the dissociation of the protonated NH_2 leaving group of the tetrahedral intermediate. However, one must consider that once protonated the intermediate collapses immediately. Additional studies must be carried out to correctly identify these two groups. At lower pH, Lys-NH_3^+ is the reactive species, whereas at higher pH, Lys-NH_2 is the reactive species. The percentage of NACs in Lys-NH_3^+ (68.3%) is double that in Lys-NH_2 (31.0%), and the corresponding free energy difference between the two reactions is only 400 cal. This is reflected in the similar barrier heights of the two bells in the pH−rate profile.

Scheme 2 affords an explanation of the pH dependence for the Pam reaction, the presence of two competing reactions dependent upon Lys110-NH_2 and Lys110-NH_3^+, and reasonable values of pK_{app} for Lys110-NH_3^+. We are aware, of course, of the fact that kinetic pK_{app} values may differ from the pK_a in water due to a change in dielectric and neighboring electrostatic effects. This would not appear to be significantly important in the Pam reaction. Also, pK_{app} may differ from pK_a due to its compound nature in mechanisms with pre- and postequilibria, but this is not a problem in the mechanism presented here (*28*).

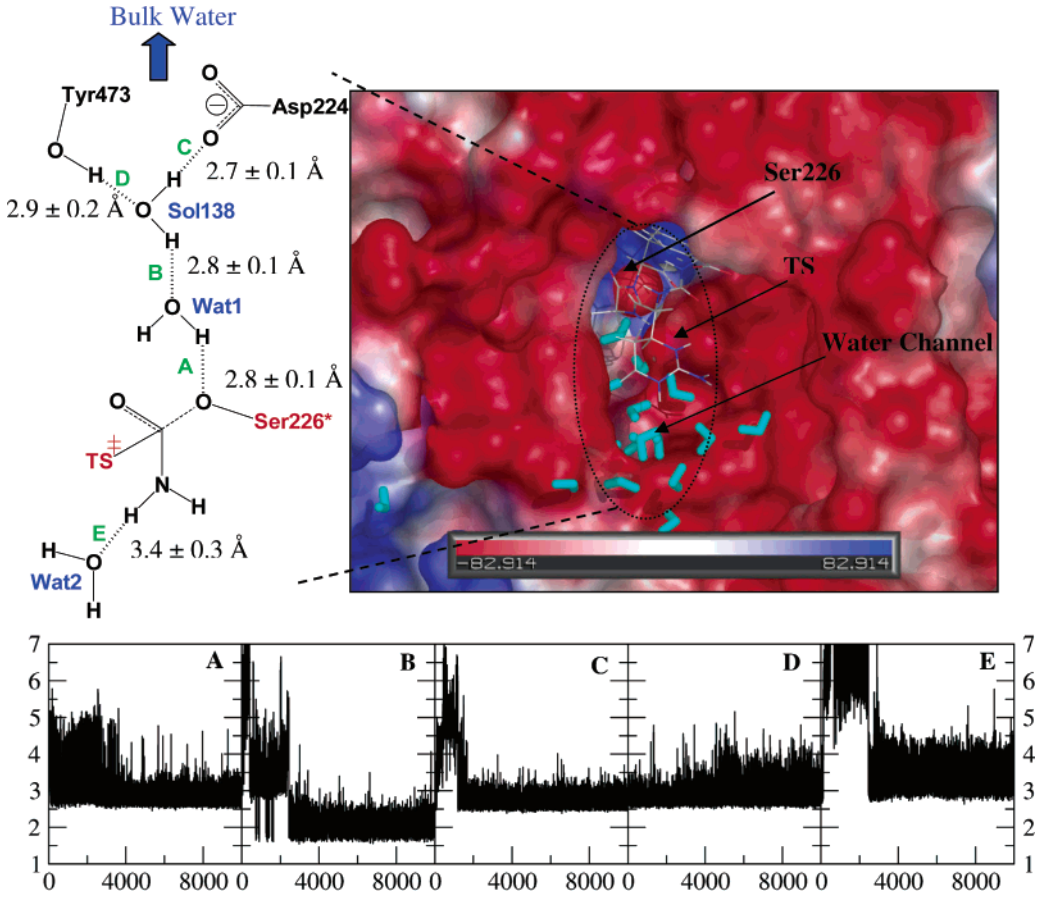

FIGURE 14: Water channel originating from Ser226 and involving the crystallographic water, Wat1. The schematic diagram (on the left) shows the positioning of the hydrogen bonds with their average distance from the MD simulation of E·TS. The three-dimensional representation of the water channel (at the right) shows Ser226 (red sphere), the TS (shown in the line diagram), and waters (shown in cyan-colored sticks) along with the rest of the protein surface (colored on the basis of the approximate electrostatic potential as generated with PYMOL). The bottom part of the figure shows the distance between the heavy atoms during the MD simulation of E·TS: (A) Ser226*−Wat1, (B) Wat1−Sol138, (C) Sol138−Asp224, (D) Sol138−Tyr473, and (E) Wat2−TS(NH_2).

Possibility of the E^-H·S Mechanism in the Pam Reaction? In the MAE2 enzyme, the pK_a of the nucleophile, Ser155 (equivalent to Ser226 in Pam), has been proposed to be lowered by the guanidine group of Arg158 being within 5.2 Å of Ser155. Thus, unlike the enzymes Pam and FAAH, the serine nucleophile (Ser155) in the MAE2 enzyme is said to be deprotonated prior to nucleophilic attack (*7*). In the Pam protein, there is no nearby guanidine group or other charged residue (<12 Å) to affect the protonation state of the side chain of Ser226-OH. The E^-H·S system has been modeled to study the positioning of Ser226-O^- if it were formed. In the E^-H·S system, *cis*-Ser202 hydrogen bonds to the negatively charged Ser226-O^-. We find that Ser226-O^- is repelled from approaching the terminal amide group of Cst-NH_2 and is stabilized some distance from the substrate. Thus, E^-H·S cannot be involved in the catalytic mechanism of Pam.

Formation of the TS in the E·S System with Lys123-NH_2. The MD simulation for the E·TS system reveals that the nucleophilic attack of Ser226 on the electrophilic carbon atom of the substrate in forming the tetrahedral intermediate is concerted with the proton transfer from Ser226-OH to Ser202-OH to Lys123-NH_2. The oxyanion hole composed of Asp224 and Thr223 backbone amides stabilizes the developing negative charge on the amide carbonyl carbon of the substrate.

Formation of the TS in the EH·S System with Lys123-NH_3^+. The structure obtained from the MD simulation of E·TS can also be seen as a possible TS formed from the EH·S system. Although the catalytic mechanism of Pam with Lys123-NH_3^+ has been proposed previously (*9*), the route of proton transfer from the nucleophilic Ser226 is not clear. We observe a narrow water channel as shown in Figure 14, leading to Ser226*. The water channel is lined with residues, such as Gly201, Gly225, Cys229, Asp224, Tyr473, and the peptide of the substrate. At the TS, Wat1 is perfectly lined up to receive a proton from Ser226* and channel it to the outside of the protein with assistance from other solvent molecules, such as Sol138 in this case (Figure 14). This water channel involving Ser226* and Wat1 might play a crucial role in increasing the nucleophilicity of Ser226*. It is worth mentioning that such a narrow water channel and an ordered hydrogen bond between Ser226* and Wat1 are present only in the E·TS system, of the five systems that have been studied. The water channel present in the E·TS system is different from one observed by X-ray crystallography (*9*) and can be seen as a unique feature of enzyme transition state stabilization. The previously reported water channel

connected Lys123 to a second smaller cavity at the protein surface (*9*). Measurements of the rate dependence with isotopically labeled water will be an important experimental method for testing the significance of this observation.

Role of the Apparent Oxyanion Hole: Stabilization of the TS and the Tetrahedral Intermediate. Throughout the MD simulations for the five systems, the backbone NH amides of Thr223 and Asp224 make contact with the amide carbonyl oxygen of Cst-NH_2. As expected, the strength of this hydrogen bond increases in conjunction with the increase in the negative charge of the terminal amide oxygen during formation of the TS and In. This arrangement resembles the "oxyanion hole" in chymotrypsin (*25*) and provides stabilization of the transition state for nucleophilic addition of Ser226-OH to the amide carbonyl of the substrate and the resultant negatively charged tetrahedral intermediate (Figure 9). A similar oxyanion hole was also observed in the MAE2 enzyme (*29*). Once the tetrahedral intermediate is formed, the amide nitrogen of the nucleophilic serine is also close enoughto hydrogen bond to the oxyanion intermediate. Thus, the three backbone amide NH groups of Ser226, Asp224, and Thr223 are hydrogen bonded to the oxyanion of the tetrahedral intermediate of the Pam reaction. In the case of the MAE2 enzyme, there are four residues (Thr152, Gly153, Gly154, and Ser155) that stabilize the negatively charged intermediate (*7*).

Collapse of the Tetrahedral Intermediate (In). As expected, protonation of the terminal NH_2 group of the substrate is not concerted with the nucleophilic addition to form the TS (see Chart 3C). During the E·TS simulation, the hydroxyl oxygen of Ser202-OH moves closer but does not hydrogen bond to the terminal amide nitrogen of Cst-NH_2. Lys123-NH_3^+ continues to remain strongly hydrogen bonded to Ser202-OH.

The trajectory for the E·In system indicates that both Ser202 and Lys123 are possible candidates that can protonate the tetrahedral NH_2 leaving group and facilitate the collapse of tetrahedral intermediate (Figure 10). The hydroxyl hydrogen of Ser202-OH makes intermittent contact with both the hydroxyl oxygen of Ser226* and the terminal amide nitrogen of the tetrahedral intermediate as shown in Figure 10. The Lys123-NH_3^+-Ser202-OH dyad can transfer a proton to the terminal NH_2 of the tetrahedral intermediate. Lys123-NH_3^+ is in position to donate a proton to Ser202-O^- such that Lys123-NH_2 and Ser202-OH return to their initial states.

On the other hand, the MD simulation of the E·In system shows that after 4 ns (refer to Figure 11C), Lys123-NH_3^+ indeed moves closer and establishes hydrogen bonding contact with the NH_2 group of the tetrahedral intermediate, suggesting an alternate path in which Lys123-NH_3^+ directly acts as a catalyst to protonate the leaving group. This may occur by pre-equilibrium proton transfer or concerted general acid catalysis. The NH_3 that is formed upon collapse of the tetrahedral intermediate can exit (as NH_3 or NH_4^+) from the active site along the water channel leading to Lys123, first described in the X-ray structure by Labahn et al. (*9*) and also observed during our MD simulation of E·In.

Ester Hydrolysis of the Acyl−Enzyme Intermediate. The MD simulation for the E·In system shows that the active site is solvent accessible. The amino nitrogen of Lys123-NH_3^+ and the tetrahedral intermediate NH_2 are hydrogen bonded to two to three water molecules, including Wat1 as shown in Figure 15. It would appear quite reasonable that the hydrolysis of the acyl−enzyme intermediate is mediated by Lys123-NH_2 general base-catalyzed water addition to the ester moiety (see Figure 16, steps D and E).

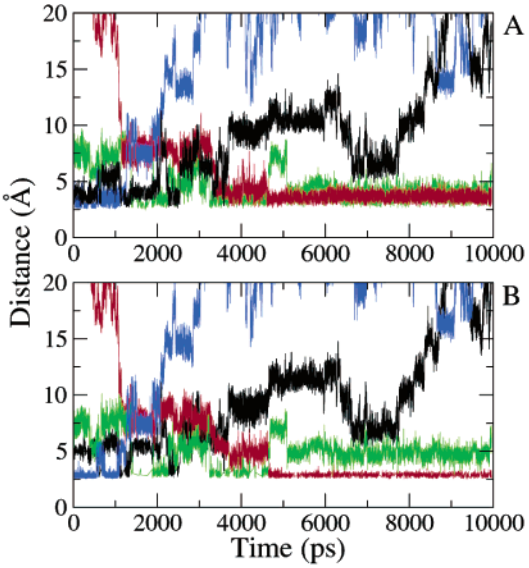

FIGURE 15: Histogram for the E·In system showing water molecules that are hydrogen bonded at certain points of the MD simulation to the (A) terminal amide nitrogen of Cst-NH_2 and (B) amino nitrogen of Lys123-NH_3^+ (red lines). Panels A and B show heavy atom distances in angstroms. The black and blue lines represent crystal water molecules (Wat1 and Wat2), and the green and red lines represent solvent water molecules.

Proposed Catalytic Mechanism for Peptide Amidase Starting with the E·S State Using Molecular Dynamics Simulation

Both the experimental pH−rate profile and the percentage of NAC determined by computational means support two mechanisms for Pam catalysis. This has led to the proposal that at lower pH Lys123-NH_3^+ is involved and at higher pH Lys123-NH_2 is involved. The latter mechanism is presented in Figure 16. The Lys123-NH_3^+ mechanism is much the same except in the TS the proton on Ser226 is being removed to the proton transfer channel consisting of ordered water molecules (Figure 14 and Chart 4). Hydrogen bonding of

Chart 4

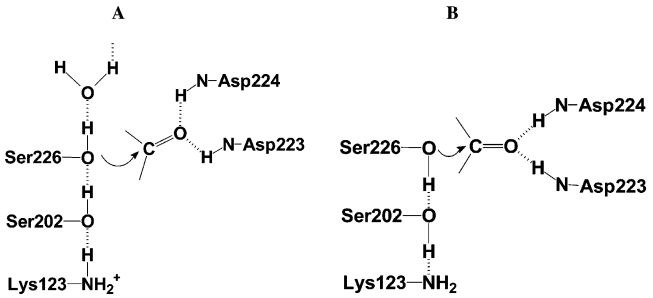

Wat1 of the channel to Ser226 in the mechanism involving Lys123-NH_2 would provide stabilization of the TS.

The biological relevance of two different mechanisms of Pam is difficult to judge since the natural function of the periplasmic Pam is not known. Considering the fact that Pam is isolated from *S. maltophilia*, a ubiquitous organism that

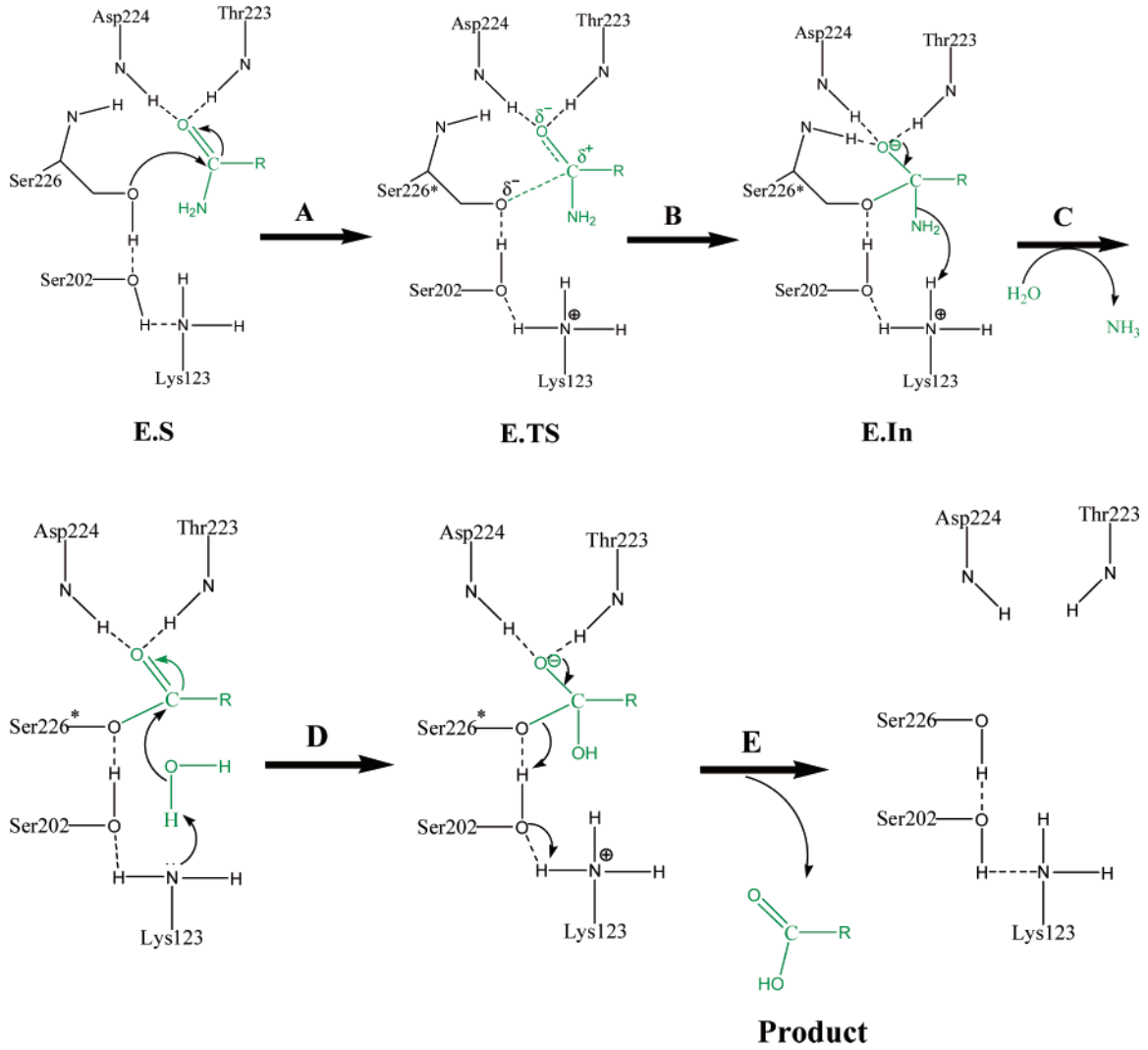

FIGURE 16: Ser-Ser-Lys catalytic triad mechanism for peptide amidase starting with the E·S state (higher pH) from MD simulations. Steps A−C have been explored computationally using MD simulations in this study, while steps D and E are suggested pathways for the formation of the carboxylic product. (A) Activation of the nucleophilic Ser226-OH. A hydrogen bonding network is observed among the highly conserved catalytic triad residues, Ser226, Ser202, and Lys123. Lys123-NH_2 functioning as a general base catalyst facilitates proton transfer through the stable hydrogen bonding network that exists among the catalytic amino acids where *cis*-Ser202-OH is the bridging ligand between the nucleophilic Ser226-OH and the final proton acceptor Lys123-NH_2. The nucleophilic addition of Ser226 to the amide carbonyl carbon atom of the substrate is concerted with the proton transfer from Ser226-OH to Ser202-OH to Lys123-NH_2. The electrophilic character of the amide carbon atom is enhanced by the hydrogen bond interactions between the terminal amide carbonyl oxygen of the substrate and the amide hydrogens atoms of Asp224 and Thr223. (B) Formation of the tetrahedral intermediate (E·In) and the oxyanion hole. The amide nitrogens of Asp224 and Thr223 create an oxyanion hole by strongly hydrogen bonding to the terminal amide oxygen of the substrate, stabilize the TS, and form the tetrahedral intermediate. In the intermediate state (E·In), the amide nitrogen of Ser226* is within good hydrogen bonding distance of the oxyanion species. (C) Collapse of the tetrahedral intermediate. Lys123-NH_3^+ protonates the NH_2 entity of the tetrahedral intermediate, releasing NH_3 and regenerating the neutral Lys-NH_2. (D) Ester hydrolysis of the acyl−enzyme intermediate. A water molecule approaches and partakes in the hydrolysis of the resultant ester linkage of the covalent acyl−enzyme intermediate, with Lys123 general-base catalysis. (E) Formation of the product. The hydrolysis reaction results in the release of a carboxylic product, allowing the catalytic triad residues to return to their original state.

is found in a wide variety of environments, it is not surprising that more than one pH-dependent pathway exists. One might imagine that the two bell-shaped curves give it a broader range of activity since the reaction rates vary very little in the pH range of 6−11.

ACKNOWLEDGMENT

We acknowledge the National Partnership for Advanced Computational Infrastructure (NPACI) for their generous allocation of the computational resources at the AMD clusters at the University of Michigan Supercomputing Center. We are grateful to Prof. Joachim Granzin for sharing the pH profile for Pam. We thank Dr. Sun Hur for her help.

REFERENCES

1. Mayaux, J. F., Cerbelaud, E., Soubrier, F., Yeh, P., Blanche, F., and Petre, D. (1991) Purification, cloning, and primary structure of a new enantiomer-selective amidase from a *Rhodococcus* strain: Structural evidence for a conserved genetic cloning with nitrile hydratase, *J. Bacteriol. 173*, 6694−6704.
2. Chebrou, H., Bigey, F., Arnaud, A., and Galzy, P. (1996) Study of the amidase signature group, *Biochim. Biophys. Acta 1298*, 285−293.
3. Dodson, G., and Elodawer, A. (1998) Catalytic triads and their relatives, *Trends Biochem. Sci. 23*, 347−352.

4. Patricelli, M. P., and Cravatt, B. F. (2000) Clarifying the catalytic roles of conserved residues in the amidase signature family, *J. Biol. Chem. 275*, 19177−19184.
5. Patricelli, M. P., Lovato, M. A., and Cravatt, B. F. (1999) Chemical and Mutagenic Investigations of Fatty Acid Amide Hydrolase: Evidence for a Family of Serine Hydrolases with Distinct Catalytic Properties, *Biochemistry 38*, 9804−9812.
6. Patricelli, M. P., and Cravatt, B. F. (1999) Fatty acid amide hydrolase competively degrades bioactive amides and esters through a nonconventional catalytic mechanism, *Biochemistry 38*, 14125−14130.
7. Shin, S., Young, S. Y., Hyun, M. K., Yu, S. K., Kwan, Y. C., and Oh, B.-H. (2003) Characterization of a Novel Ser-cisSer-Lys Catalytic Triad in Comparison with the Classical Ser-His-Asp Triad, *J. Biol. Chem. 278*, 24937−24943.
8. McKinney, M. K., and Cravatt, B. F. (2003) Evidence for Distinct Roles in Catalysis for Residues of the Serine-Serine-Lysine Catalytic Triad of Fatty Acid Amide Hydrolase, *J. Biol. Chem. 278*, 37393−37399.
9. Labahn, J., Neumann, S., Buldt, G., Kula, M.-R., and Granzin, J. (2002) An Alternative Mechanism for Amidase Signature Enzymes, *J. Mol. Biol. 322*, 1053−1064.
10. Schwarz, A., Wandrey, C., Steinke, D., and Kula, M.-R. (1992) A two-step enzymatic synthesis of dipeptides, *Biotechnol. Bioeng. 39*, 132−140.
11. Bradbury, A. F., and Smyth, D. G. (1987) Biosynthesis of the C-terminal amide in peptide hormones, *Biosci. Rep. 7*, 907−916.
12. Brooks, B. R., Bruccoleri, R. E., Olafson, B. D., States, D. J., Swaminathan, S., and Karplus, M. (1983) CHARMM: A program for macromolecular energy, minimization and dynamics calculations, *J. Comput. Chem. 4*, 187−217.
13. Brünger, A. T., and Karplus, M. (1988) Polar hydrogen positions in proteins: Empirical energy placement and neutron-diffraction comparison, *Proteins 4*, 148.
14. Frisch, M. J., Trucks, G. W., Schlegel, H. B., Scuseria, G. E., Robb, M. A., Cheeseman, J. R., Zakrzewski, V. G., Montgomery, J. A., Stratmann, R. E., Burant, J. C., Dapprich, S., Millam, J. M., Daniels, A. D., Kudin, K. N., Strain, M. C., Farkas, O., Tomasi, J., Barone, V., Cossi, M., Cammi, R., Mennucci, B., Pomelli, C., Adamo, C., Clifford, S., Ochterski, J., Petersson, G. A., Ayala, P. Y., Cui, Q., Morokuma, K., Malick, D. K., Rabuck, A. D., Raghavachari, K., Foresman, J. B., Cioslowski, J., Ortiz, J. V., Stefanov, B. B., Liu, G., Liashenko, A., Piskorz, P., Komaromi, I., Gomperts, R., Martin, R. L., Fox, D. J., Keith, T., Al-Laham, M. A., Peng, C. Y., Nanayakkara, A., Gonzalez, C., Challacombe, M., Gill, P. M. W., Johnson, B., Chen, W., Wong, M. W., Andres, J. L., Gonzalez, C., Head-Gordon, M., Replogle, E. S., and Pople, J. A. (1998) *GAUSSIAN 98*, version A.6, Guassian, Inc., Pittsburgh, PA.
15. Besler, B. H., Merz, K. M. J., and Kollman, P. A. (1990) Atomic charges derived from semiempirical methods, *J. Comput. Chem. 11*, 431−439.
16. Ryckaert, J. P., Ciccotti, G., and Berendsen, H. J. C. (1977) Numerical integration of the Cartesian equations of motion of a system with constraints: molecular dynamics of N-alkanes, *J. Comput. Phys. 23*, 327−341.
17. Verlet, L. (1967) Computer experiments on classical fluids, *Phys. Rev. 159*, 98−113.
18. Berendsen, H. J. C., Postma, J. P. M., Van Gunsteren, W. F., DiNola, A., and Haak, J. R. (1984) Molecular-dynamics with coupling to an external bath, *J. Chem. Phys. 81*, 3684−3690.
19. Brooks, C. L., III, and Karplus, M. (1989) Solvent effects on protein motion and protein effects on solvent motion, *J. Mol. Biol. 208*, 159−181.
20. Brooks, C. L., III, and Karplus, M. (1983) Deformable Stochastic Boundaries in Molecular Dynamics, *J. Chem. Phys. 79*, 6312−6325.
21. Bruice, T. C. (2002) A View at the Millennium: The Efficiency of Enzymatic Catalysis, *Acc. Chem. Res. 35*, 139−148.
22. Bruice, T. C., and Benkovic, S. J. (2000) Chemical basis for enzyme catalysis, *Biochemistry 39*, 6267−6274.
23. Li, A.-J., and Nussinov, R. (1998) A Set of van der Waals and Coulombic Radii of Protein Atoms for Molecular and Solvent-Accessible Surface Calculation, Packing Evaluation, and Docking, *Proteins: Struct., Funct., Genet. 32*, 111−127.
24. Reddy, S. Y., and Bruice, T. C. (2003) In Silico Studies of the Mechanism of Methanol Oxidation by Quinoprotein Methanol Dehydrogenase, *J. Am. Chem. Soc. 125*, 8141−8150.
25. Tsukada, H., and Blow, D. M. (1985) Structure of α-chymotrypsin at 1.68 Å resolution, *J. Mol. Biol. 184*, 703−713.
26. Neumann, S. (2002) Die Peptidamidase aus Stenotrophomonas maltophilia, Ph.D. Thesis, Heinrich-Heine Universtat, Dusseldorf, Germany.
27. Bruice, T. C., and Benkovic, S. J. (1969) pH-Rate Profiles, in *Bioorganic Mechanisms*, Vol. I, Chapter 1, pp 4−16, W. A. Benjamin, New York.
28. Bruice, T. C., and Schmir, G. L. (1959) The influence of mechanism on the apparent pK_a' of participating groups in enzymic reactions, *J. Am. Chem. Soc. 81*, 4552−4560.
29. Shin, S., Lee, T.-H., Ha, N.-C., Koo, H. M., Kim, S.-y., Lee, H.-S., Kim, Y. S., and Oh, B.-H. (2002) Structure of malonamidase E2 reveals a novel Ser-cis-Ser-Lys catalytic triad in a new serine hydrolase fold that is prevalent in nature, *Eur. Mol. Biol. Org. 21*, 2509−2516.

BI049025R